



RADIOPROPAGAÇÃO

Radio Wave Propagation

Mobile radio communications

Carlos A. Cardoso Fernandes



1. *Introduction*

1.1 Mobile communications





1. Introduction

1.2 Mobile radio services

Satellite coverage

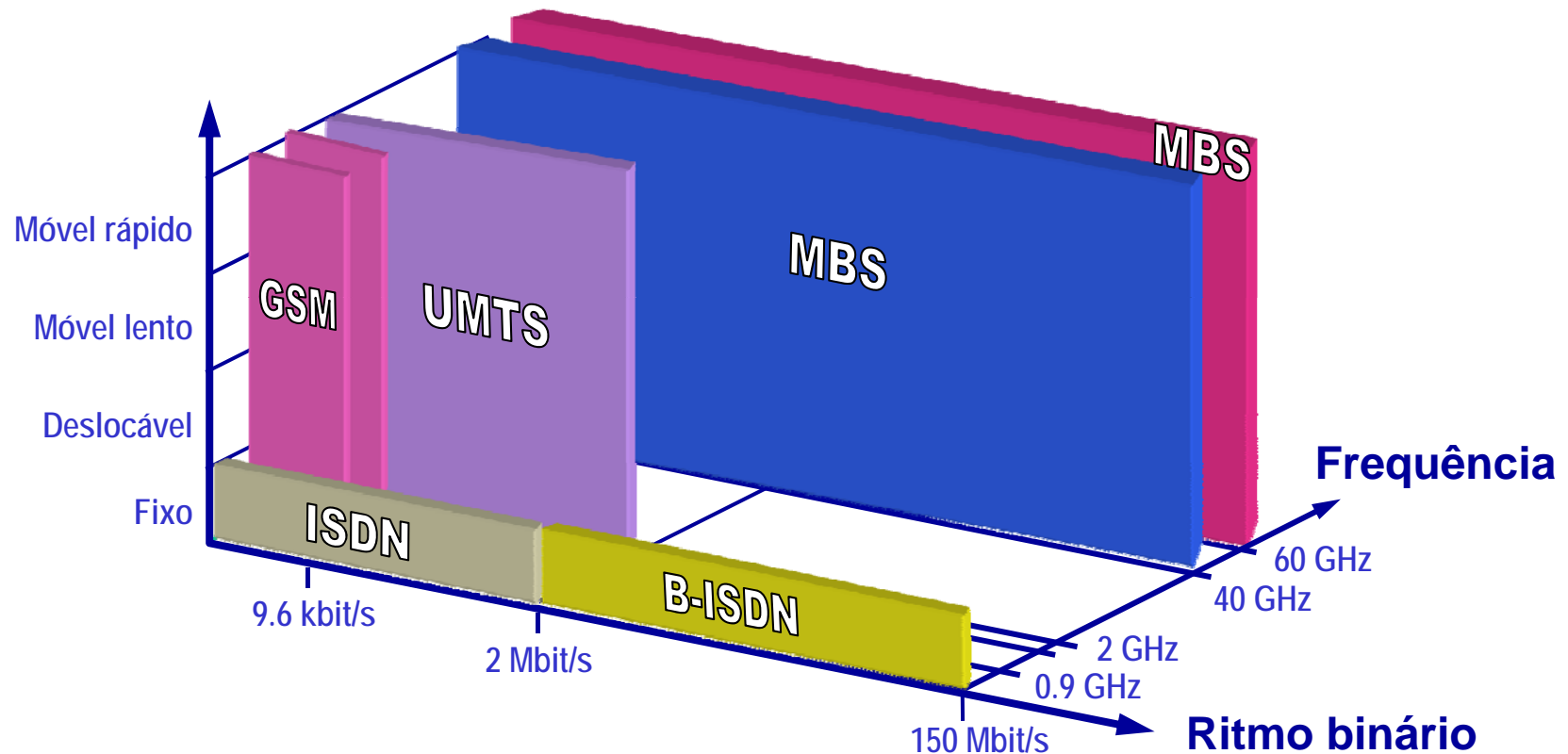
- **Aeronautical Mobile Satellite Services (AMSS)**
- **Maritime Mobile Satellite Services (MMSS)**
- **Land Mobile Satellite Services (LMSS)**

Land mobile coverage

- **GSM**
- **UMTS**
- **WI-FI, WIMAX**
- **HIPERLAN**
- **MBS**

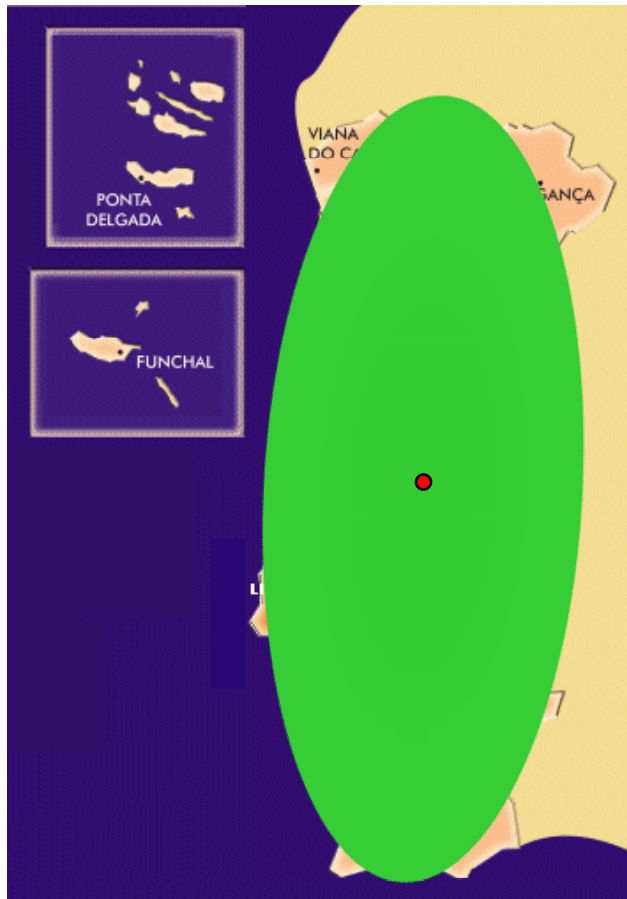
1. Introduction

1.3 Land mobile services



1. Introduction

1.4 Global coverage vs cellular coverage





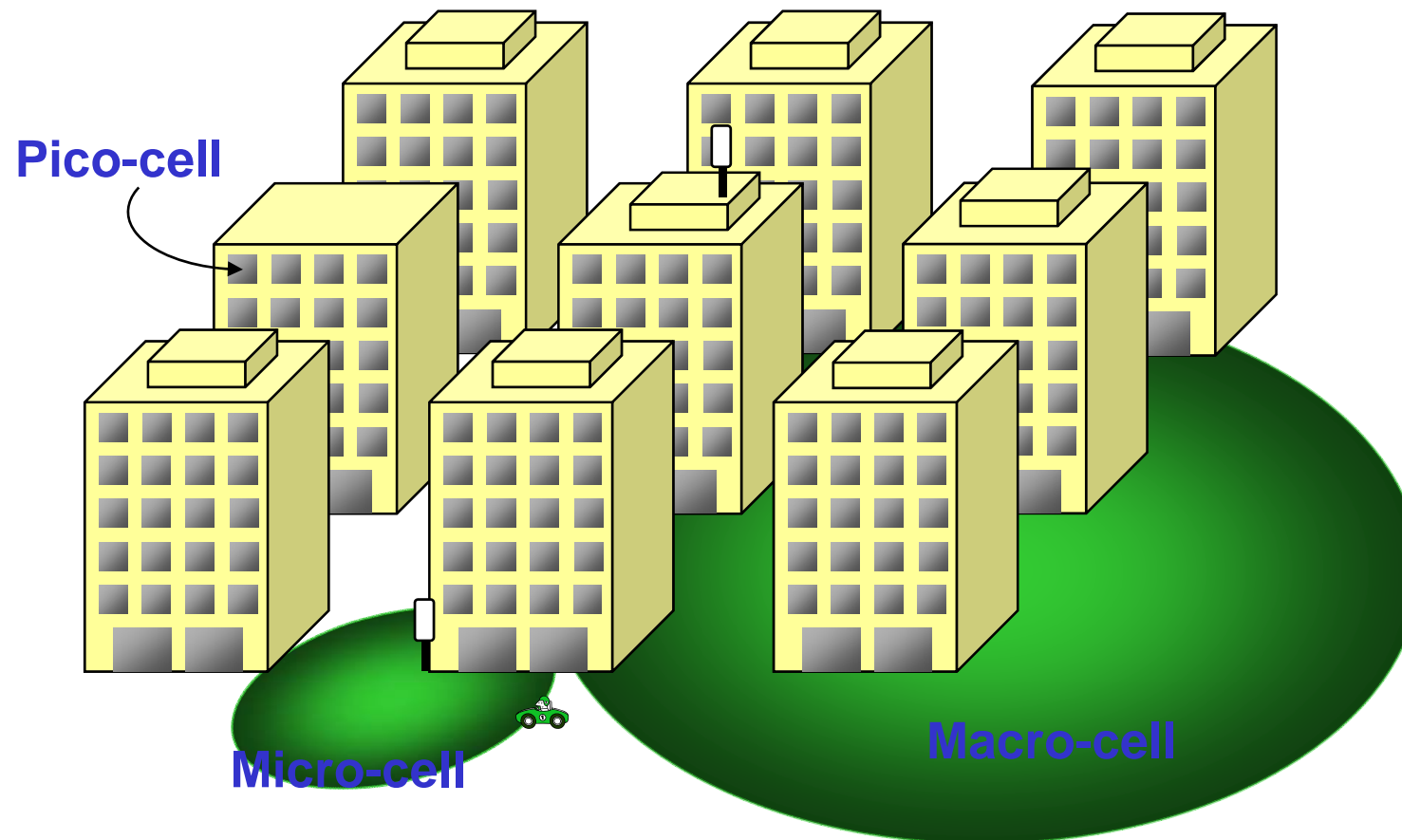
1. Introduction

1.5 Propagation modes

Cellular coverage requires accurate prediction of received signal level

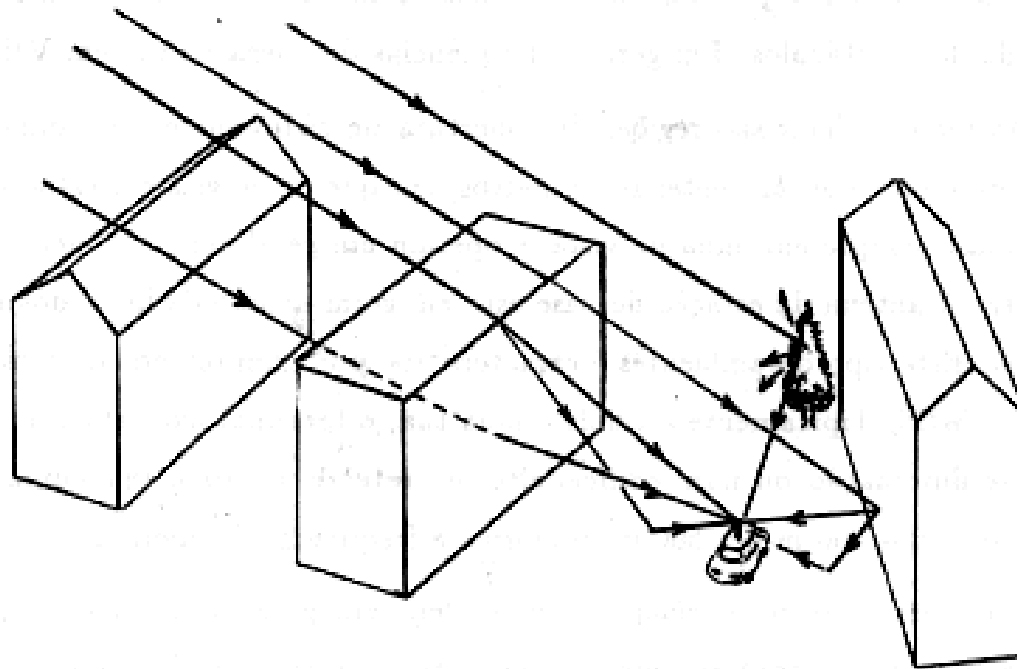
- **Deterministic models**
- **Statistical models**
- **Integrated models (estat. + determin.)**

2. Scenarios for land mobile communications



3. Specifics of land mobile scenarios

Propagation over roof-tops followed by diffraction down to street level (shadowing + multipath)



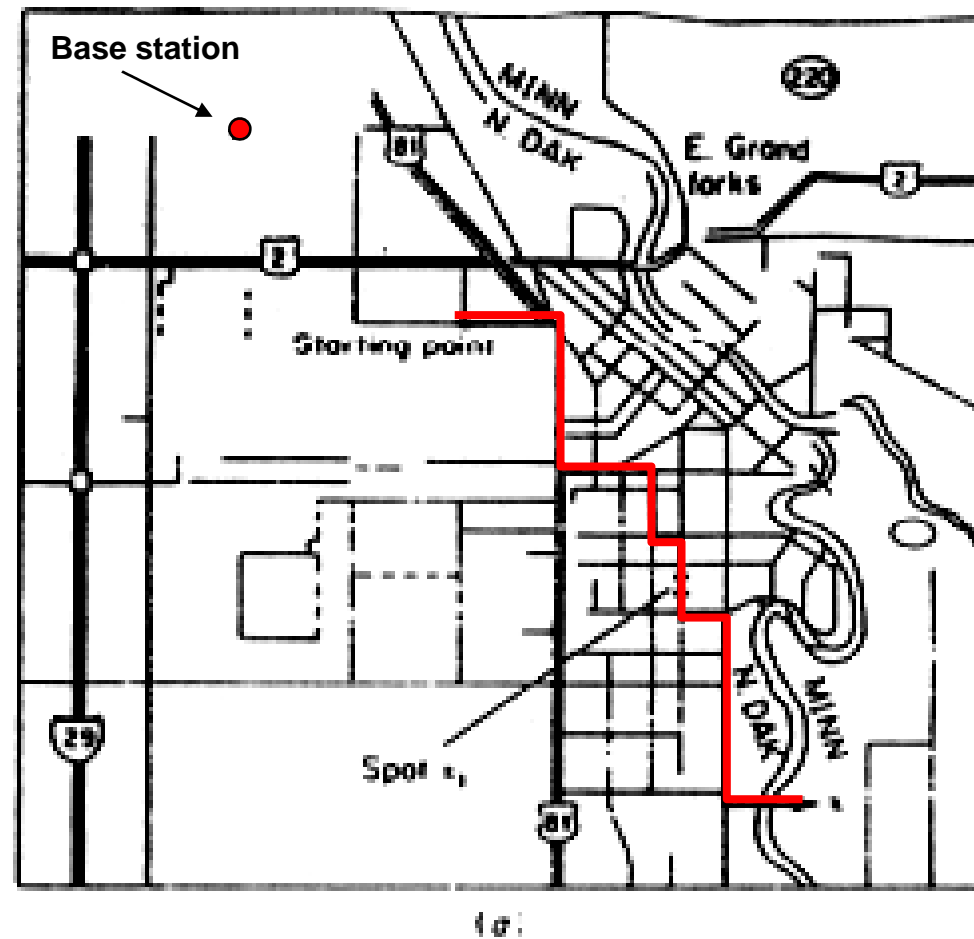
3. Specifics of land mobile scenarios

Effective scattering region slides centered with the mobile
($\sim 30 \lambda$ radius)



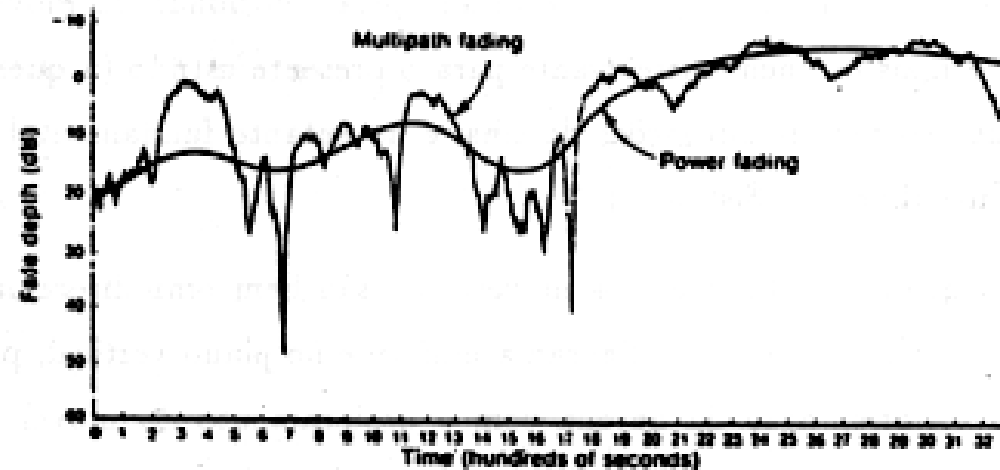
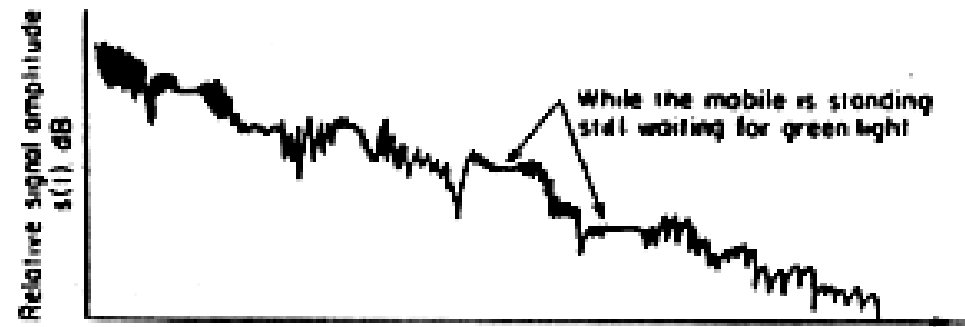
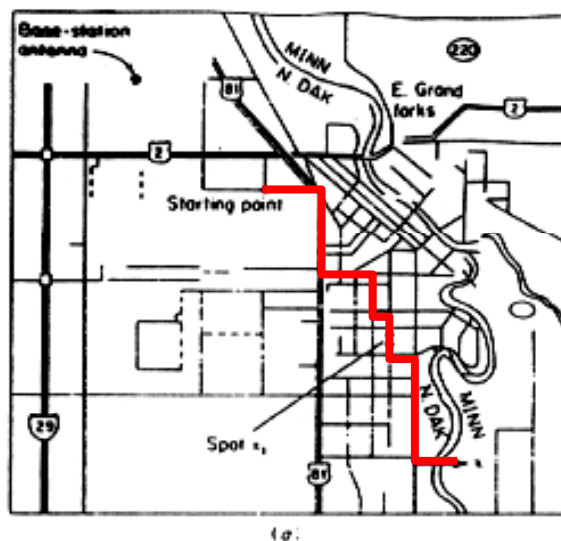
3. Specifics of land mobile scenarios

Typical urban location



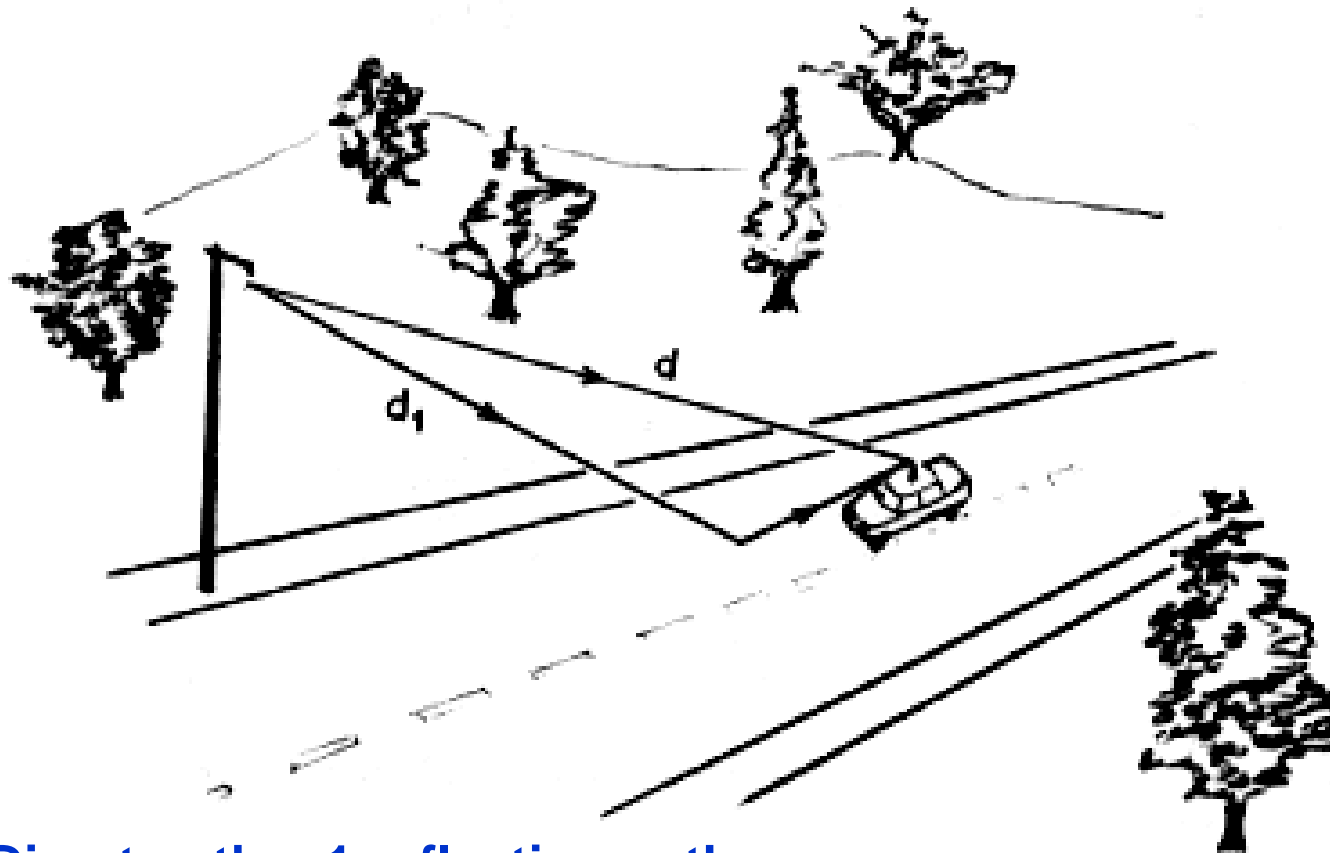
3. Specifics of land mobile scenarios

Different scales of signal level variation with distance



4. Rural micro-cell

4.1 Typical scenario

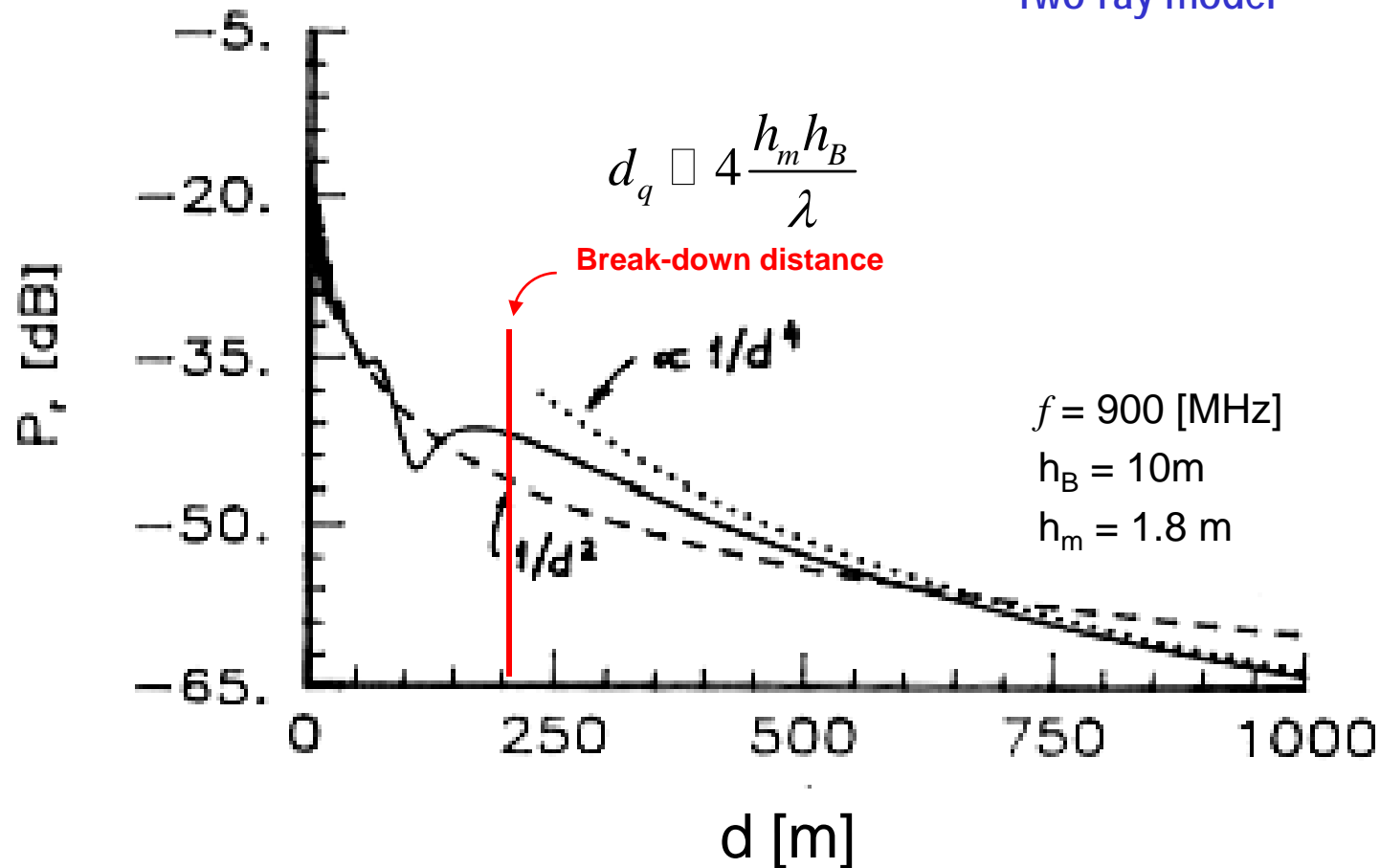


Direct path + 1 reflection path

4. Rural micro-cell

4.2 Break-down distance

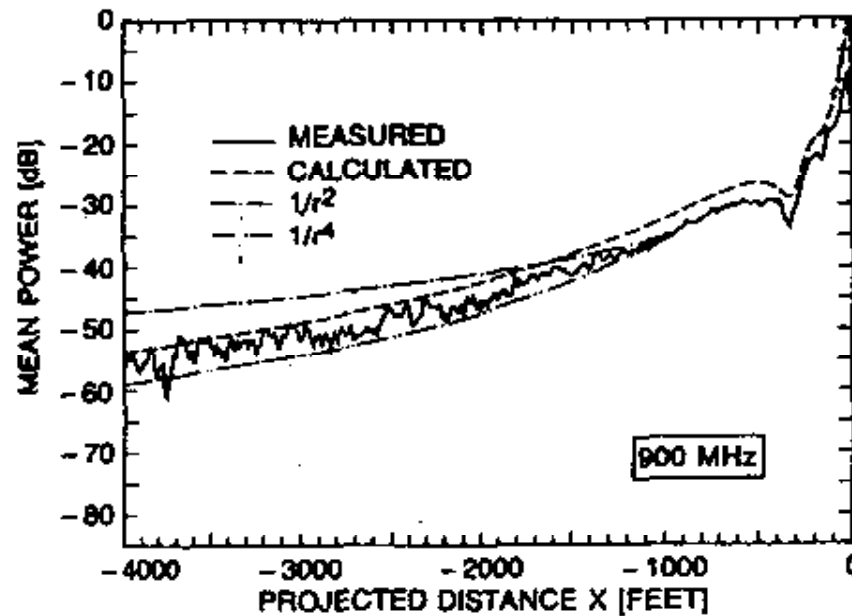
Two-ray model



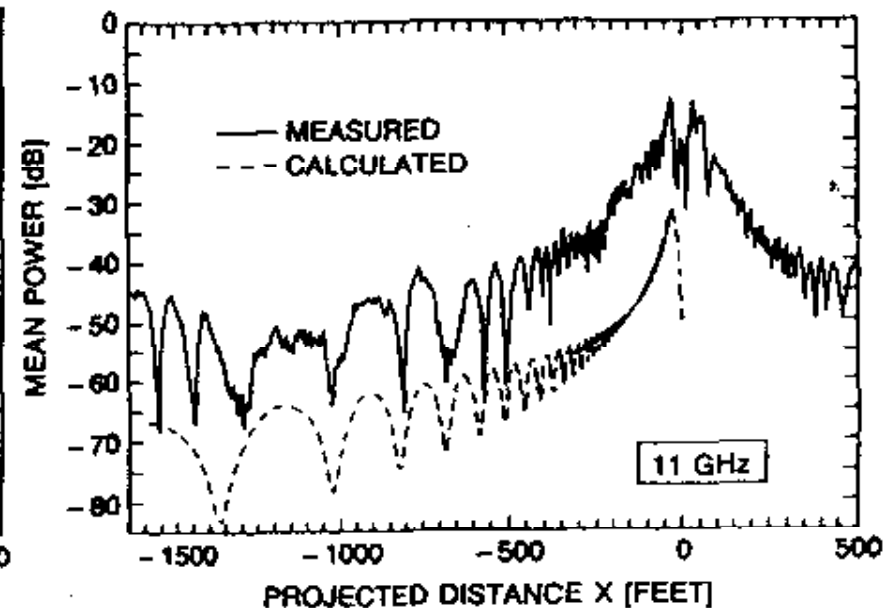
4. Rural micro-cell

4.3 Comparison with experimental results

Two-ray model



- 1200 [m] - 900 [m] - 600 [m] - 300 [m]

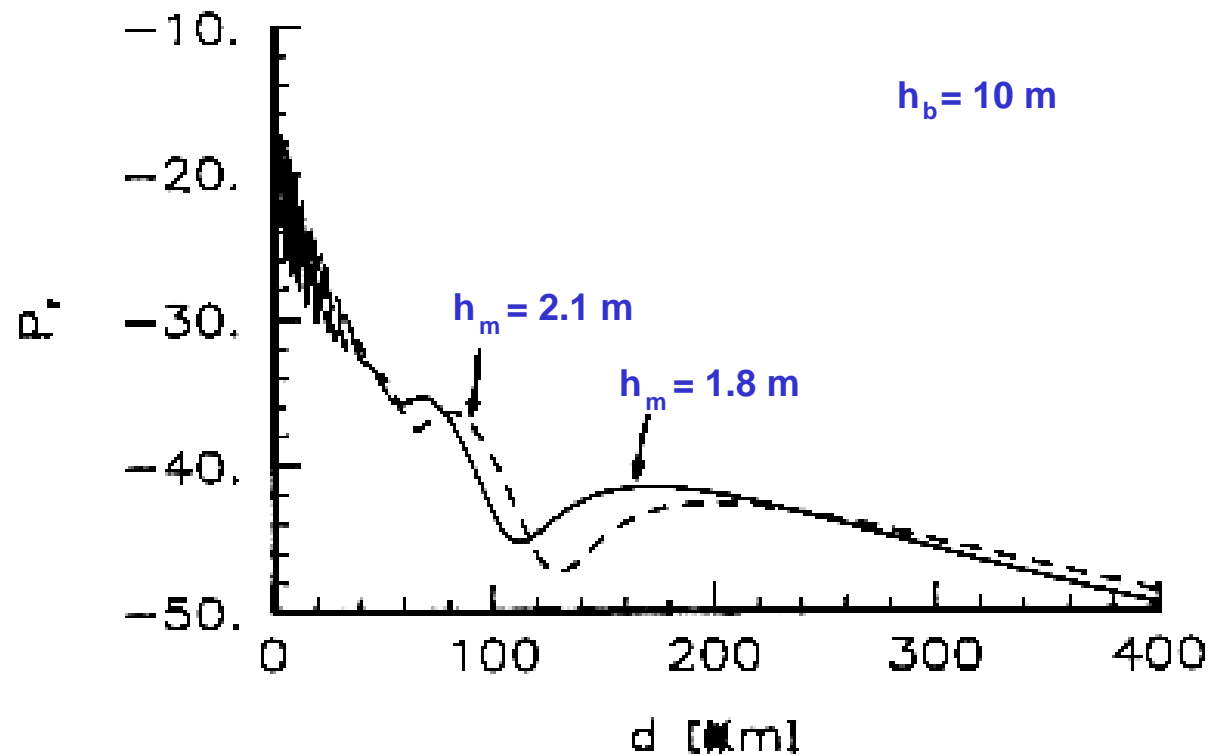


- 300 [m] - 150 [m] 150 [m]

4. Rural micro-cell

4.4 Effect of antenna height variation

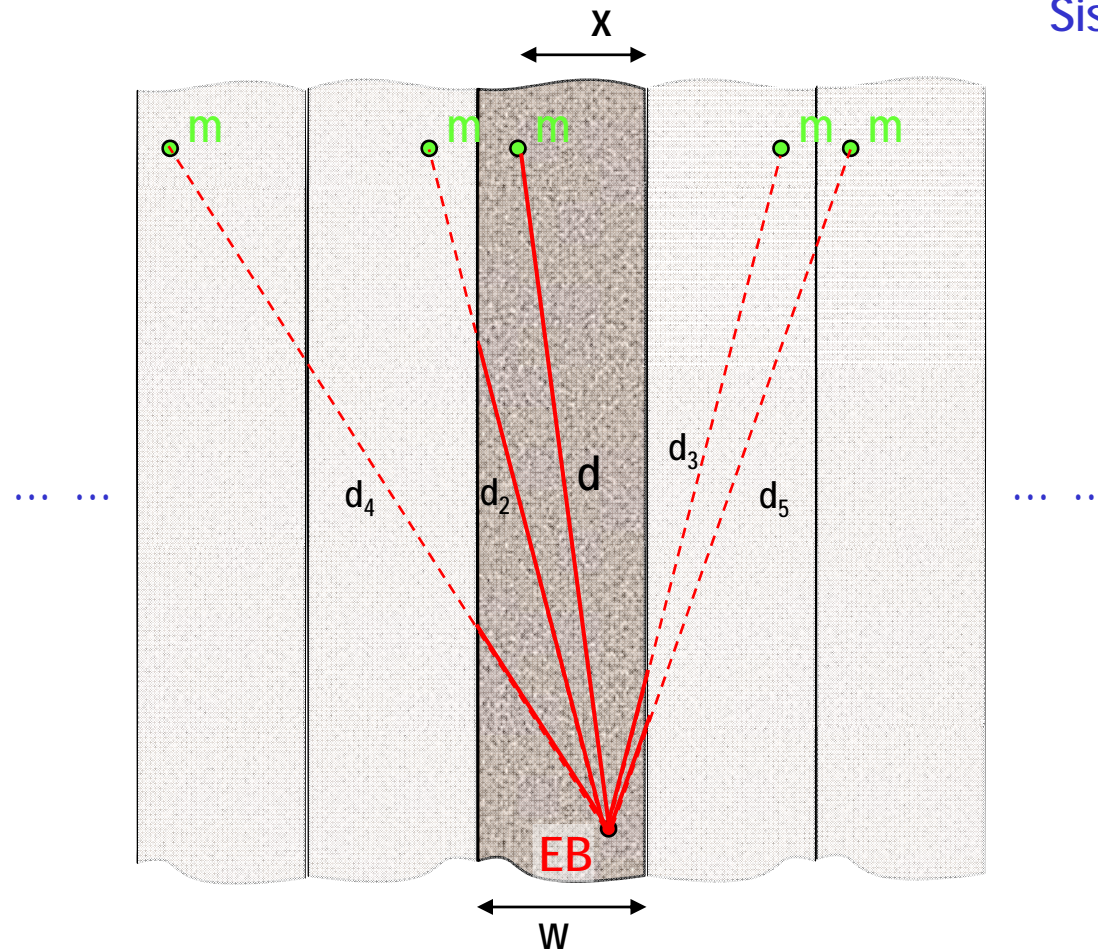
Two-ray model



5. Urban micro-cell

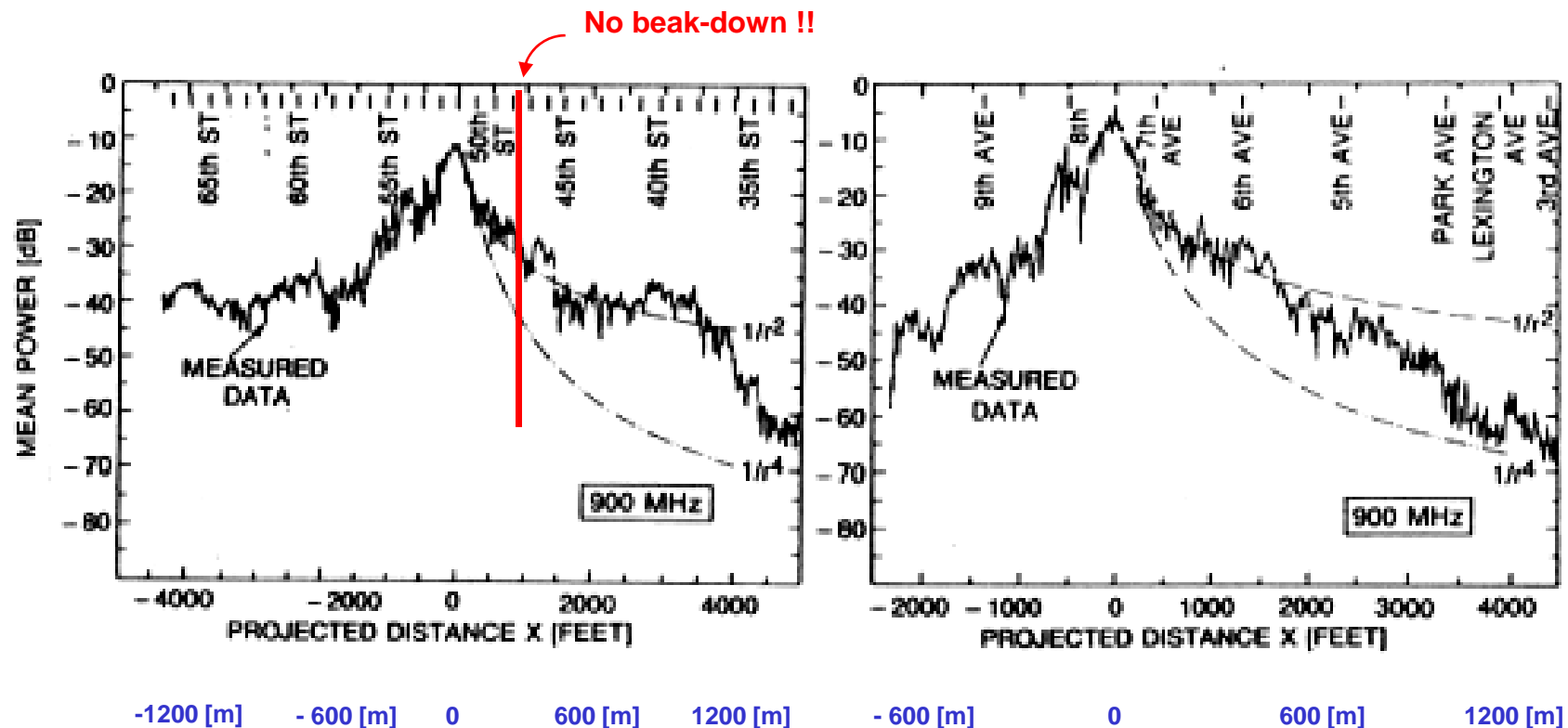
5.1 Dielectric canyon

Sis-ray model



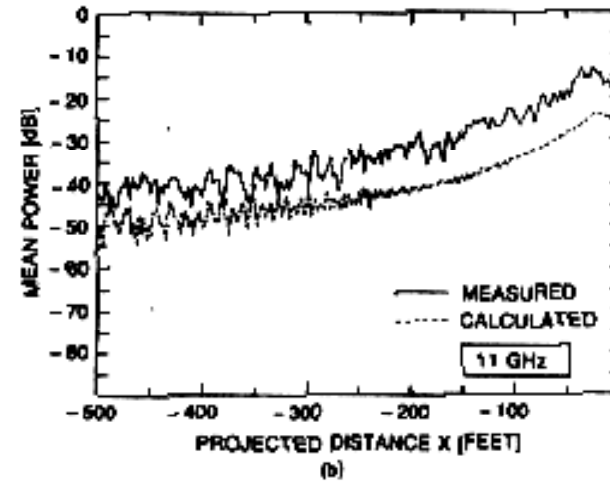
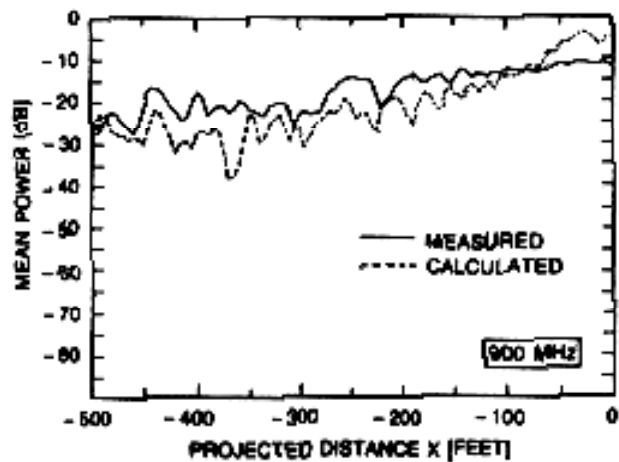
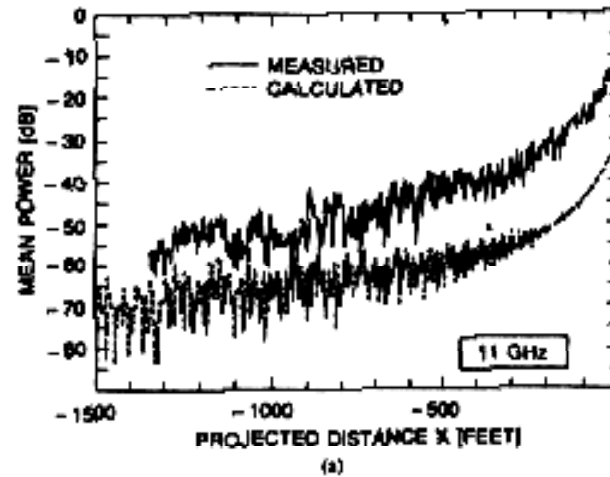
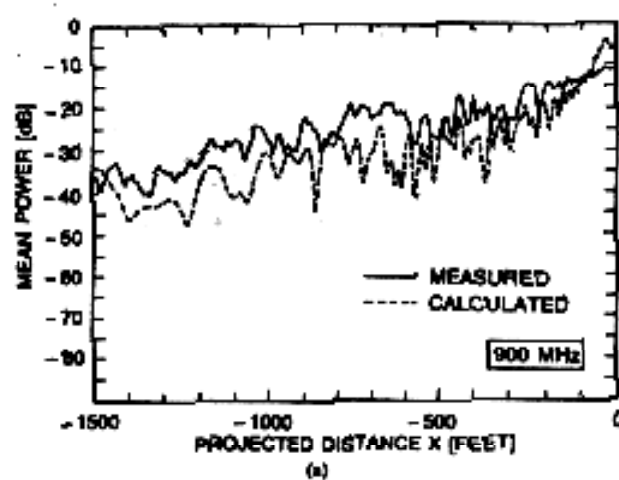
5. Urban micro-cell

5.2 Comparison with experimental results



5. Micro-célula urbana

5.2 Comparison with experimental results



Six-ray model



6. Micro-cells at mm-waves

6.1 Introduction

Applications

- Broadband mobile communications (40 or 60 GHz)
- Gigabit wireless networks (WirelessHD)

Why 60 GHz

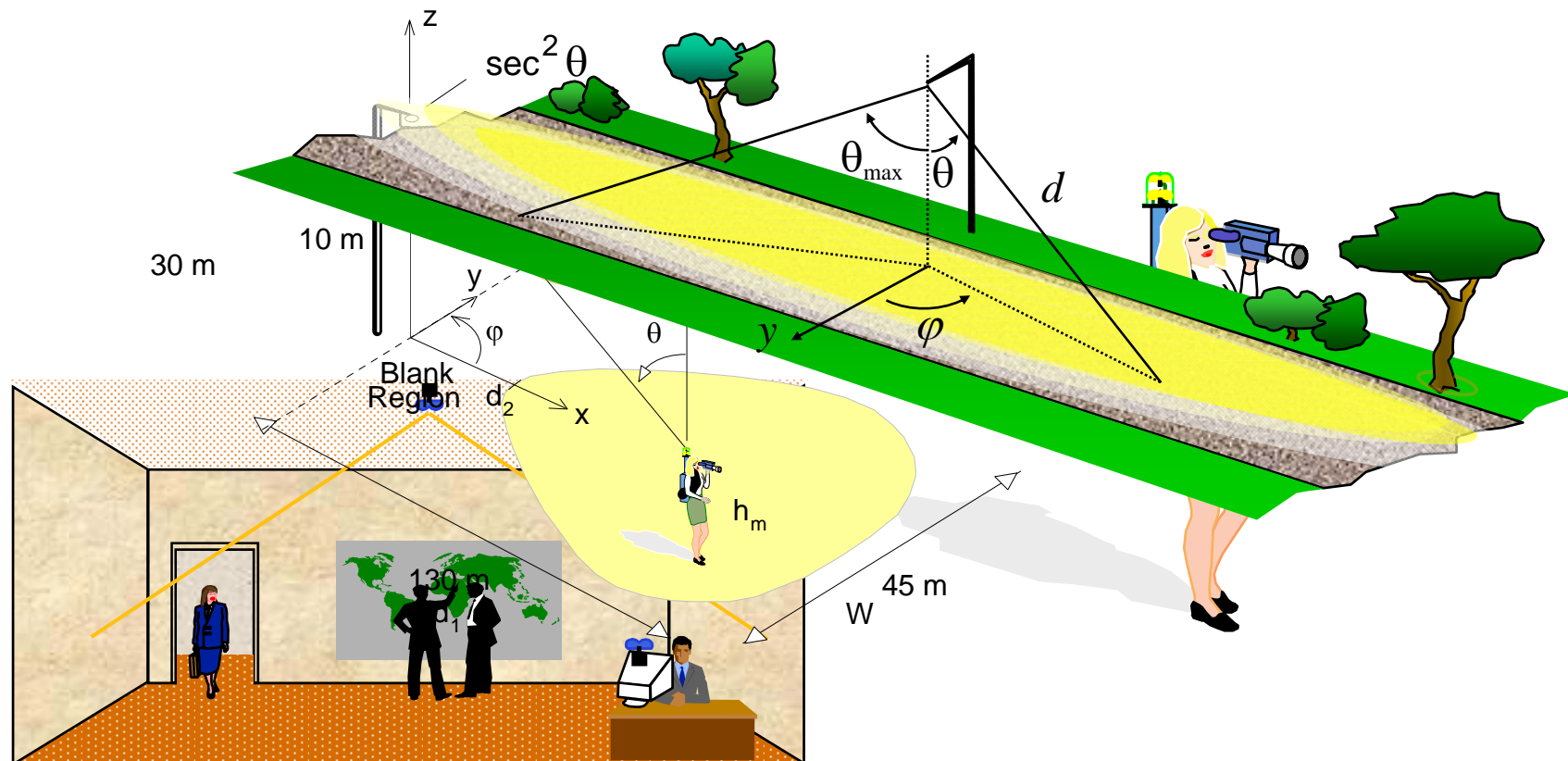
- Oxygen absorption (~ 15 dB/km)
- Spectrum availability, emerging affordable technology

Implications

- Small frequency reuse distances
- Effective EM energy confinement to the cell
- Ray models even more adequate
- Surface roughness may play a role
- Rain can be an issue (for outdoor applications)

6. Micro-cells at mm-waves

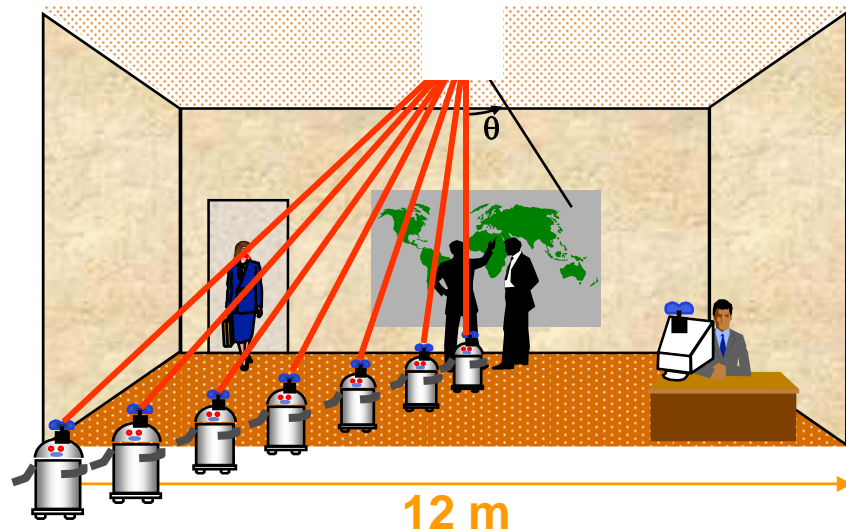
6.2 Possible scenarios



Typical cell range: 6 to 300 m

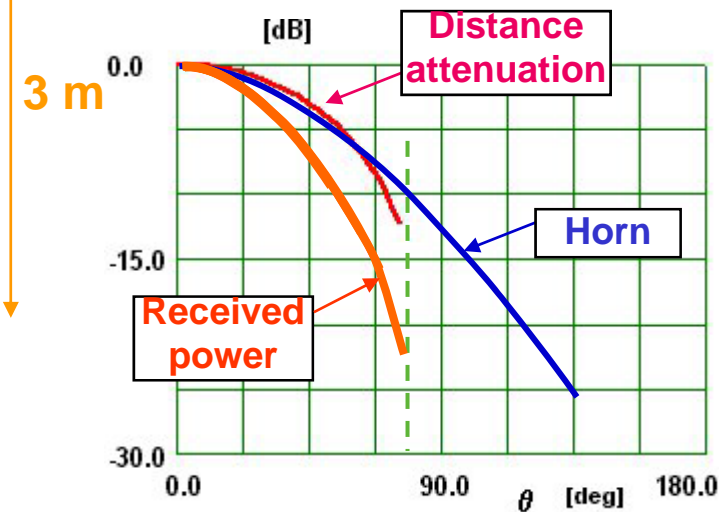
6. Micro-cells at mm-waves

6.3 Importance of antennas



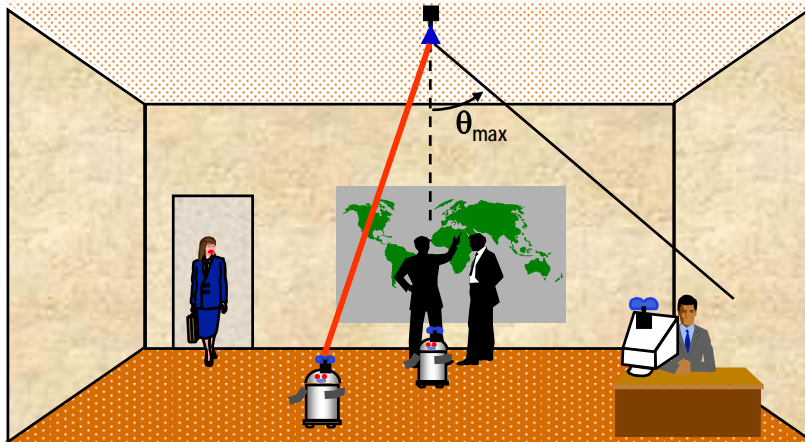
High received power dynamic range

$$P_r = P_e \frac{\lambda^2}{(4\pi)^2} \frac{G_r G_e(\theta, \varphi)}{d^2}$$



6. Micro-cells at mm-waves

6.3 Cosecant square antennas

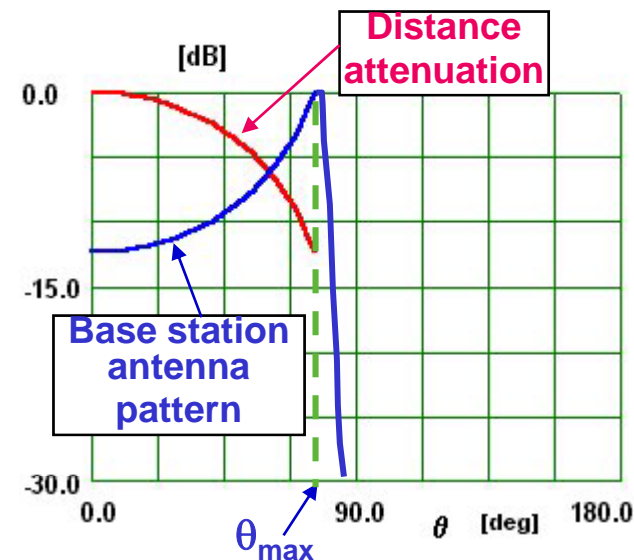


- Constant received power within the cell;

$$G_e = \sec^2 \theta = d^2 / h^2$$

- Controlled reflection from walls;

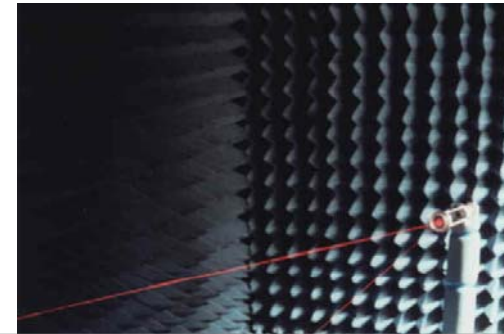
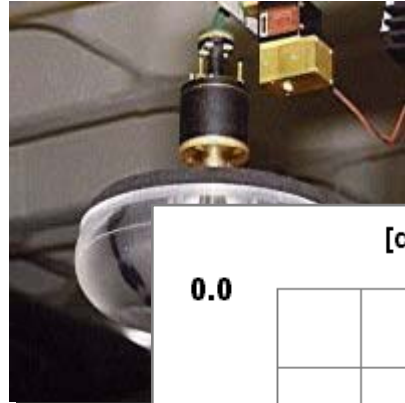
$$P_r = P_e \frac{\lambda^2}{(4\pi)^2} \frac{G_r G_e(\theta, \varphi)}{d^2}$$



6. Micro-cells at mm-waves

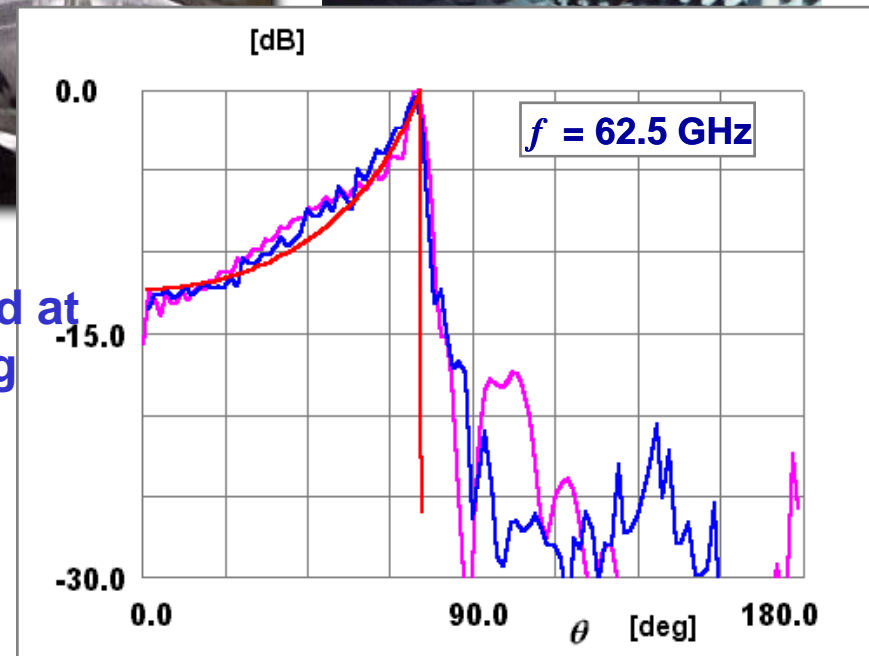
6.4 Antenna examples

New concept developed at IST



Lenses can be produced at low-cost by moulding

— Target
— Measured
— Simulation



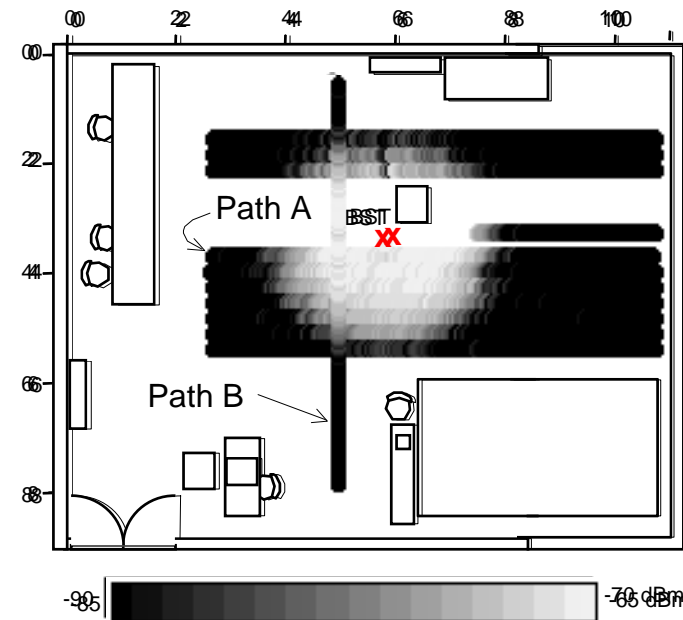
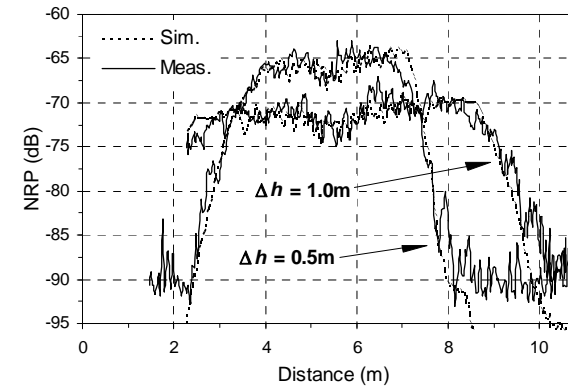
6. Micro-cells at mm-waves

6.5 Typical coverage of these antennas



$f = 62.5 \text{ GHz}$

- Cell edge is very sharp.
- Cell radius is proportional to antenna height.

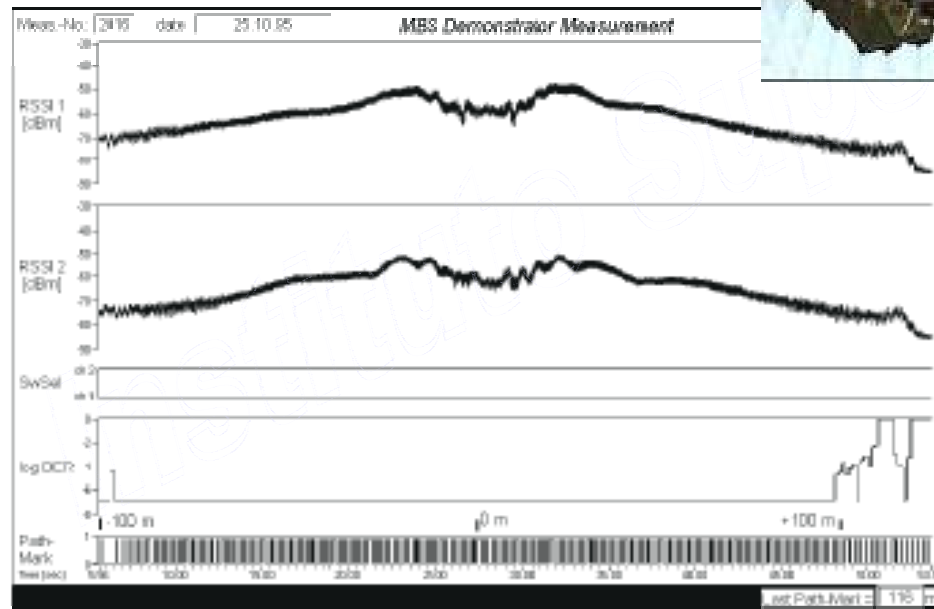


6. Micro-cells at mm-waves

6.6 MBS project

(Mobile Broadband Systems)

Cosecant square antennas
developed at IST



Public demonstration, ULM Germany, 1996

6. *Micro-cells at mm-waves*

6.6 SAMBA project

System for Advanced Mobile
Broadband Applications



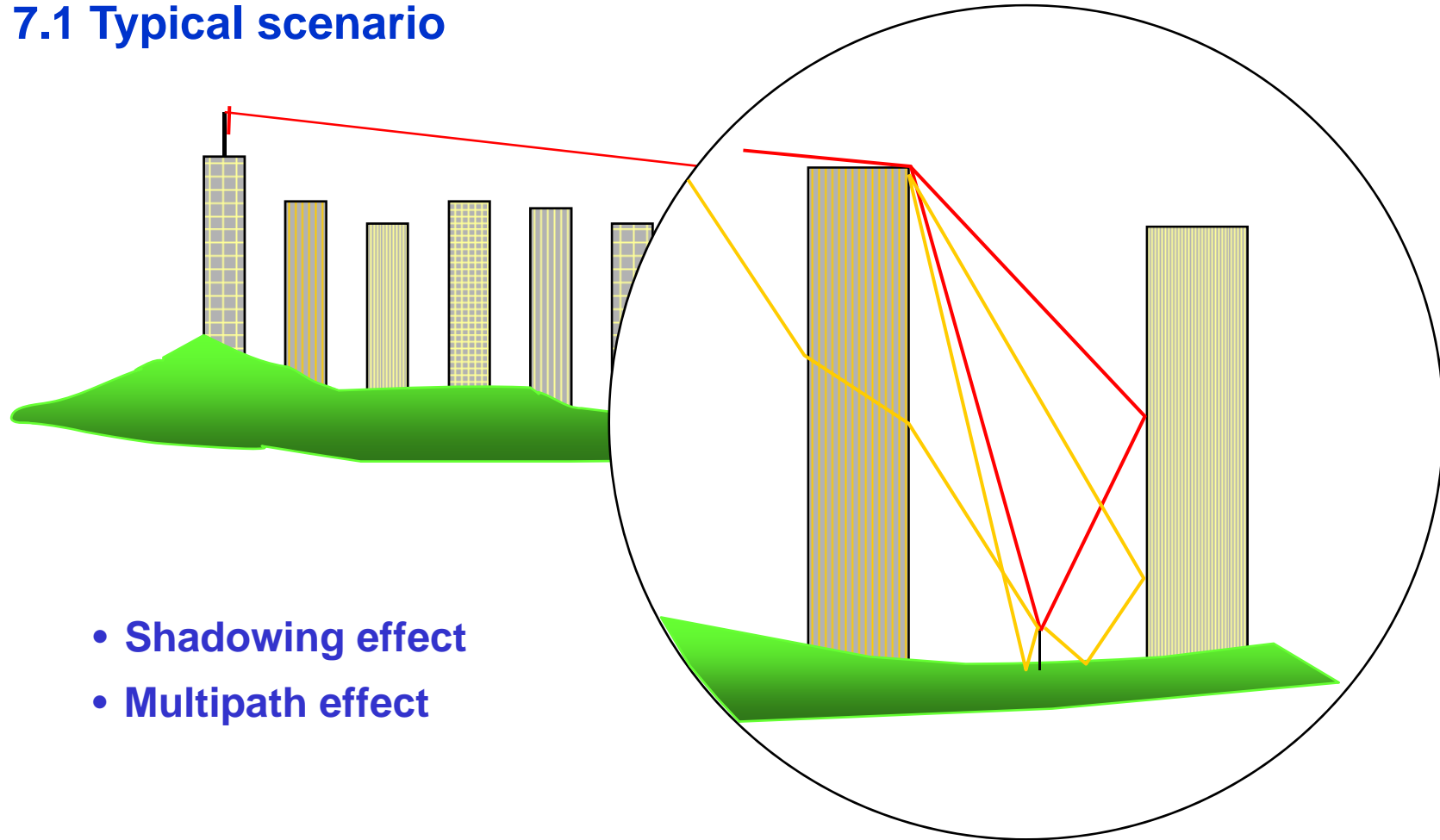
Cosecant square antennas developed at IST



Public demonstration at Utopia Pavillion,
EXPO 98, Lisboa
(Pavilhão Atlântico)

7. Macro-cells

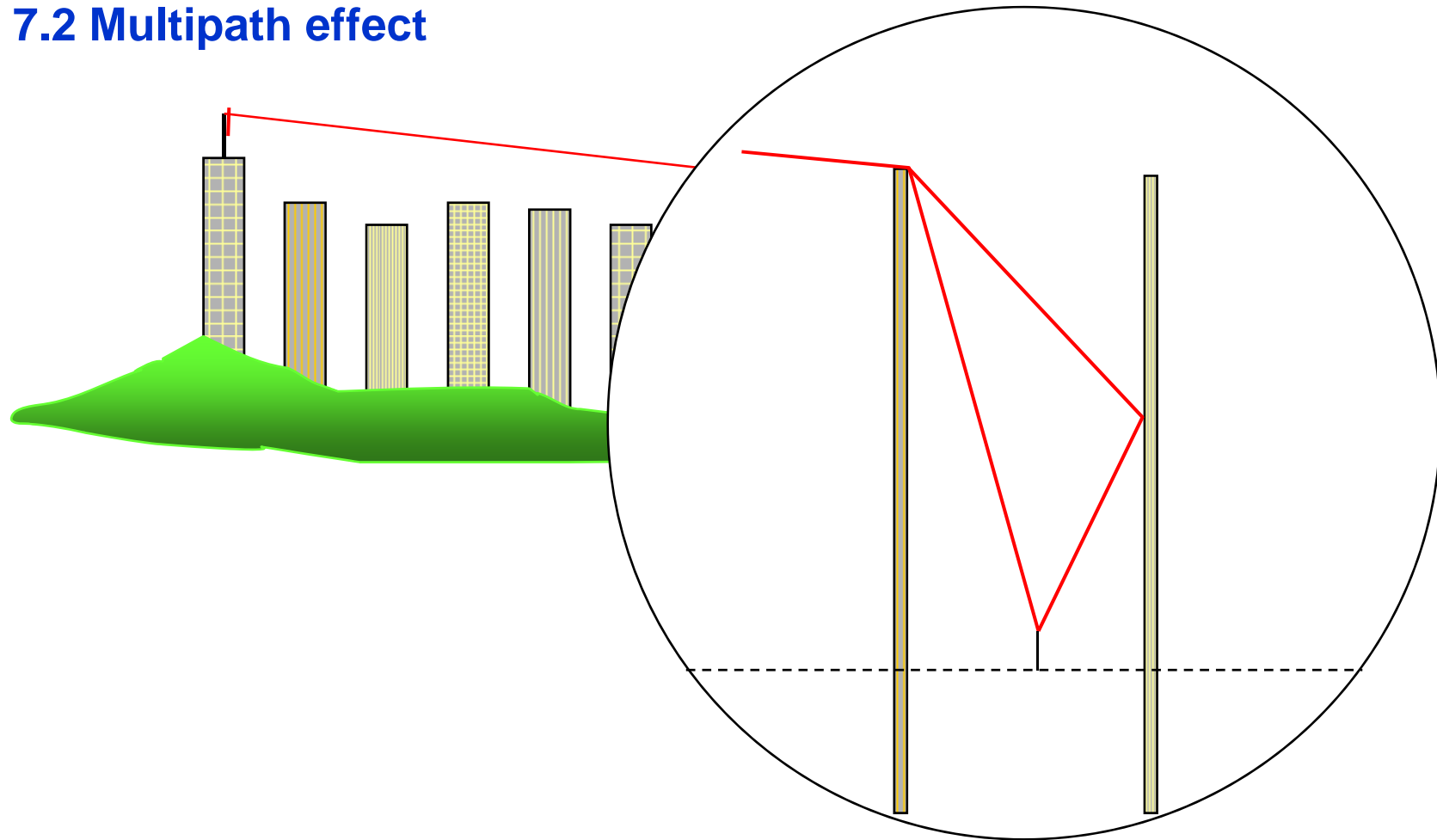
7.1 Typical scenario



- Shadowing effect
- Multipath effect

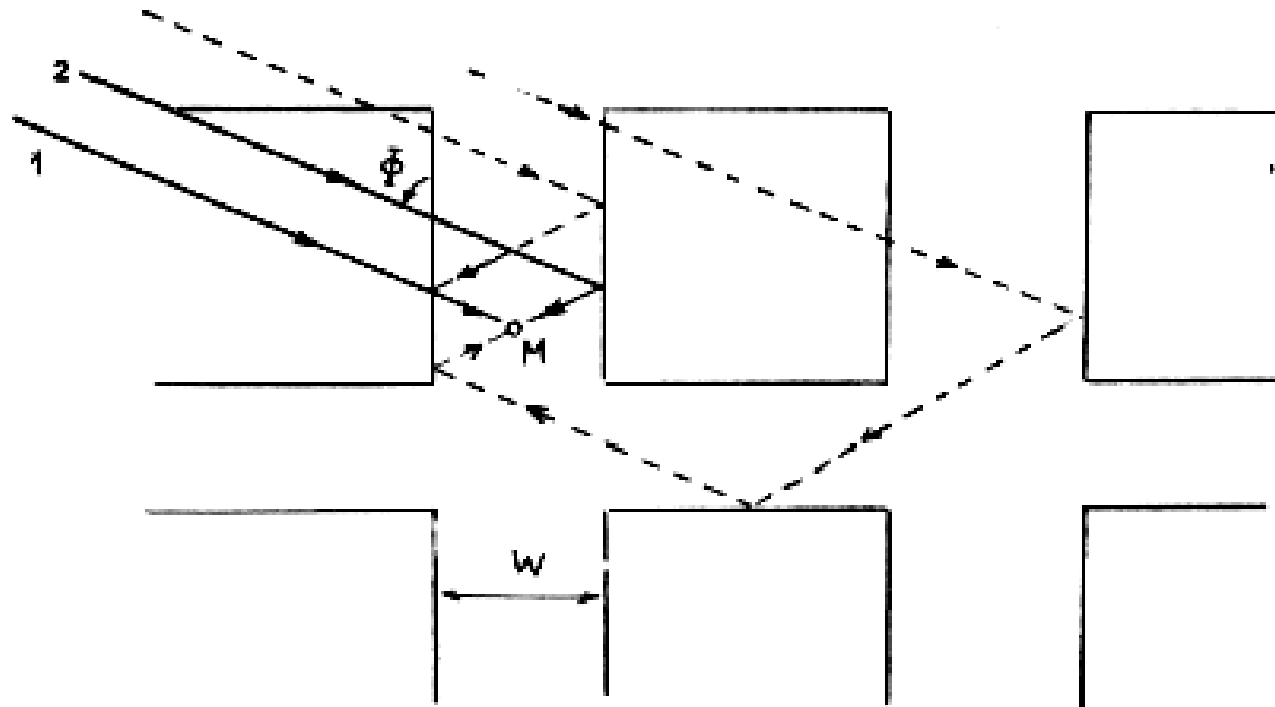
7. Macro-cells

7.2 Multipath effect



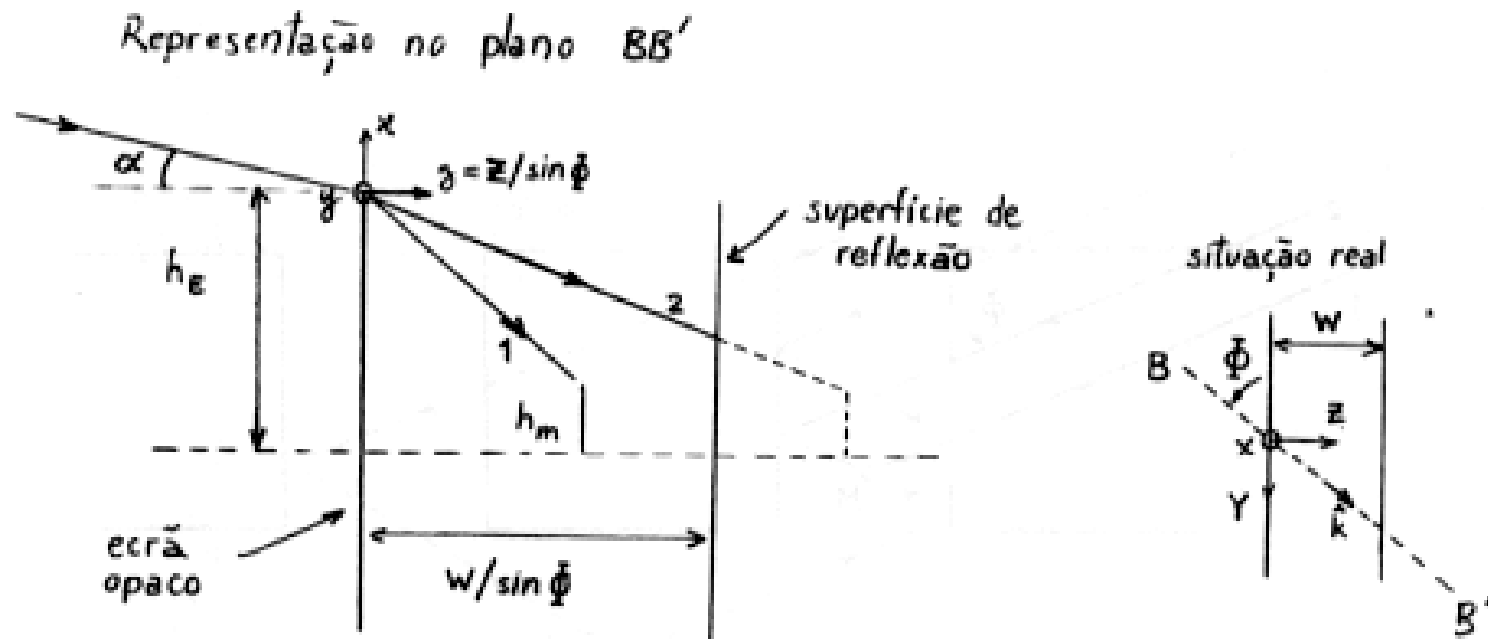
7. Macro-cells

7.2 Multipath effect



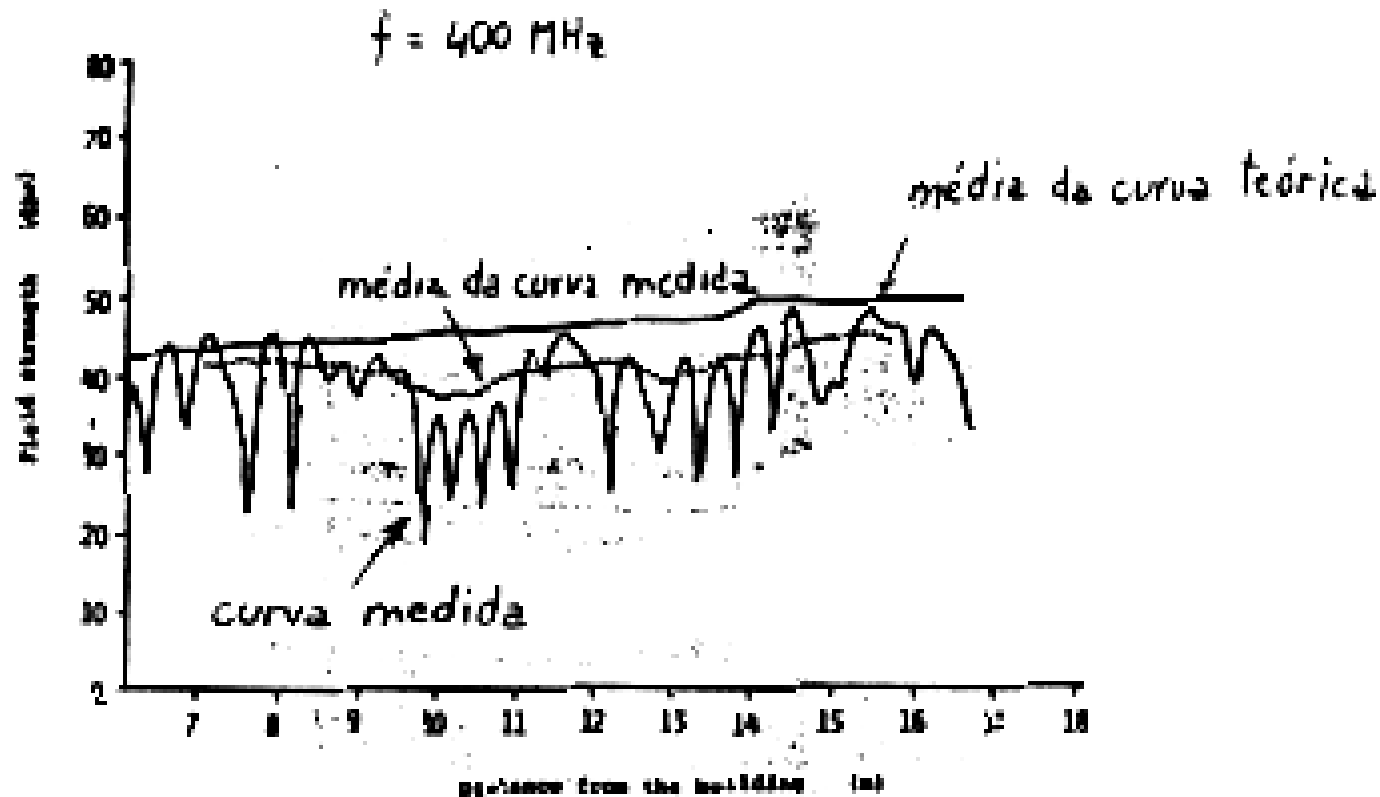
7. Macro-cells

7.2 Multipath effect



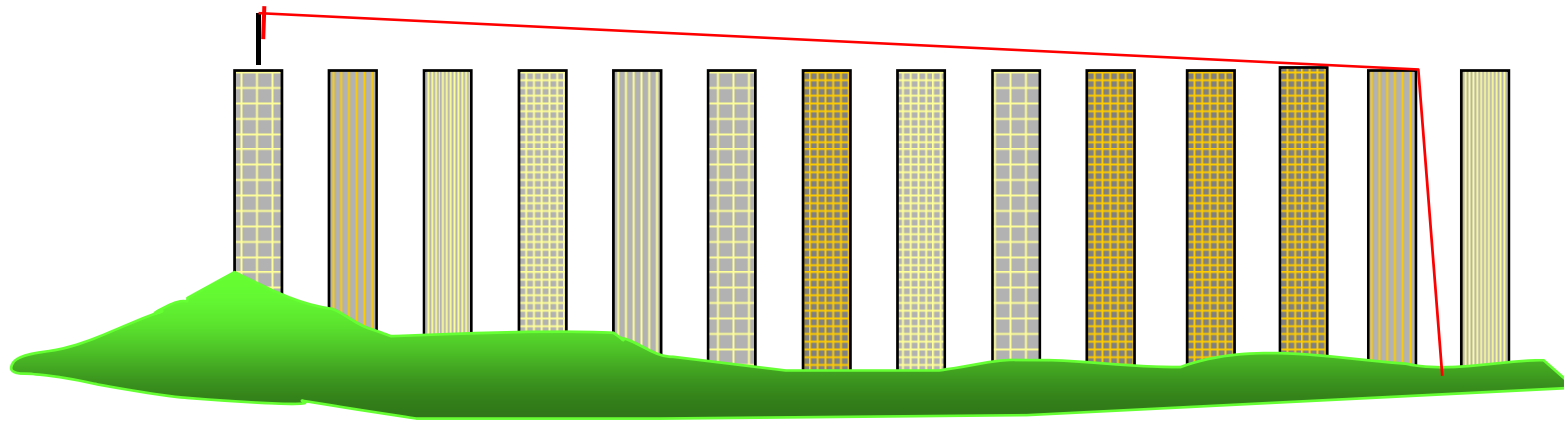
7. Macro-cells

7.2 Multipath effect



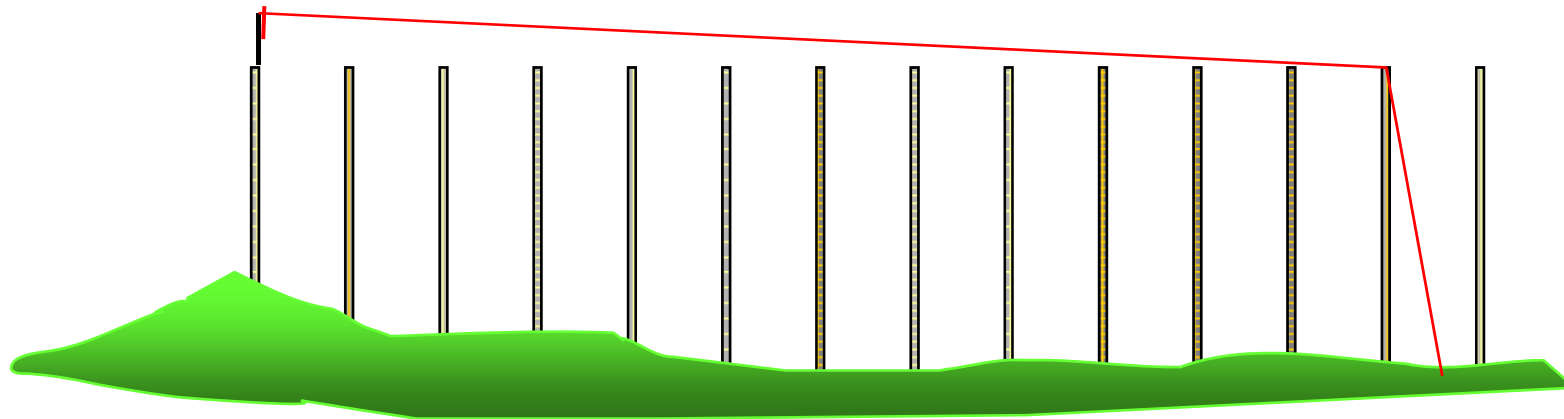
7. Macro-cells

7.3 Shadowing effect



7. Macro-cells

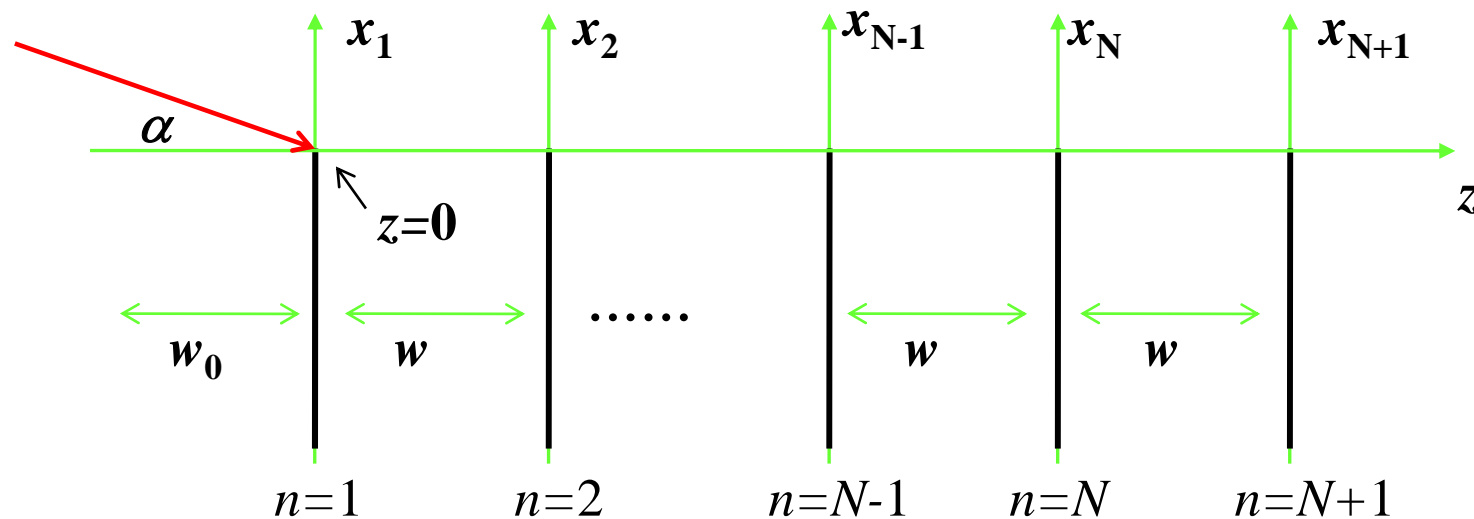
7.3 Staggered knife-edge obstacles



7. Macro-cells

7.4 Xia and Bertoni multi-obstacle attenuation model

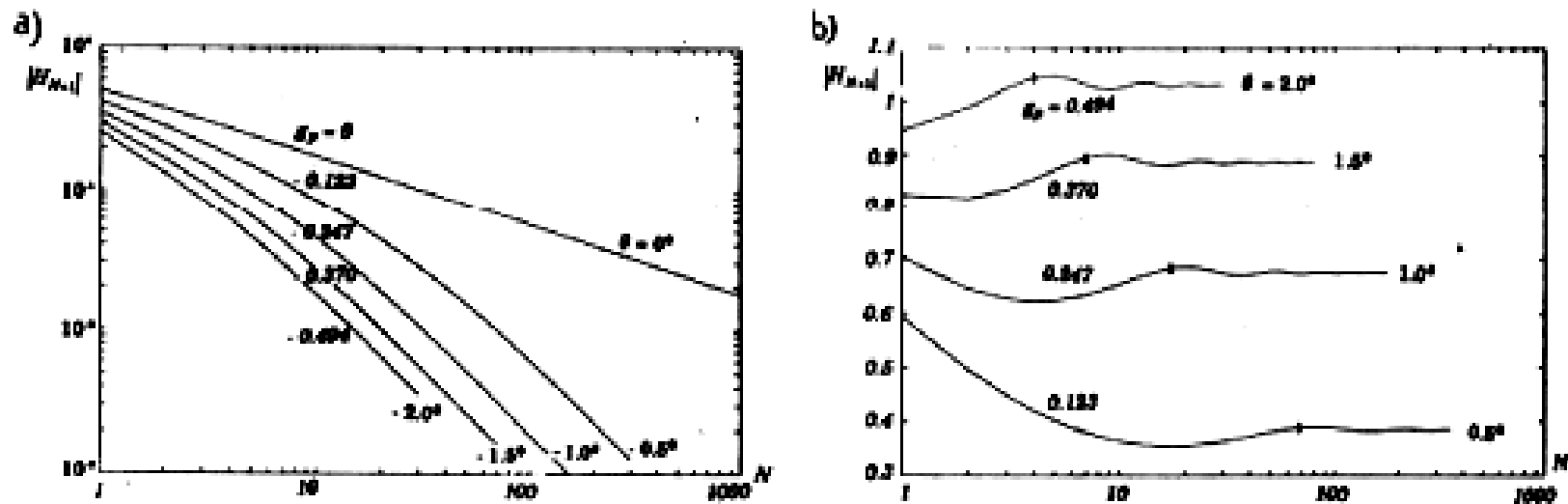
← Base station side



7. Macro-cells

7.4 Xia and Bertoni multi-obstacle attenuation model

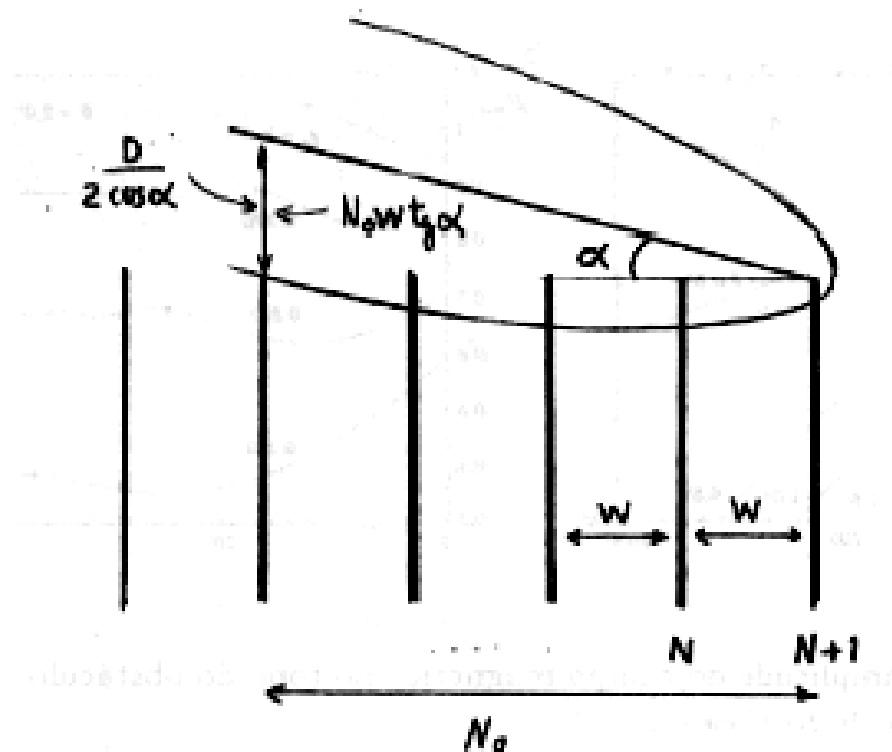
Attenuation function vs number of obstacles



7. Macro-cells

7.4 Xia and Bertoni multi-obstacle attenuation model

Interpretation of attenuation settling behaviour



7. Macro-cells

7.4 Xia and Bertoni multi-obstacle attenuation model

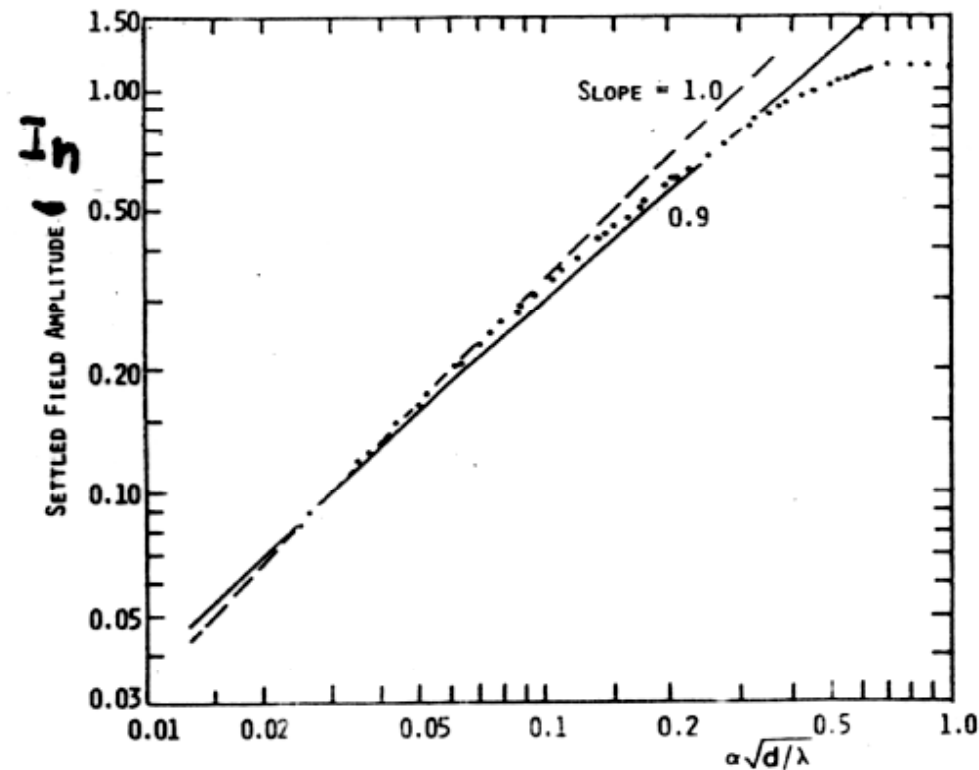
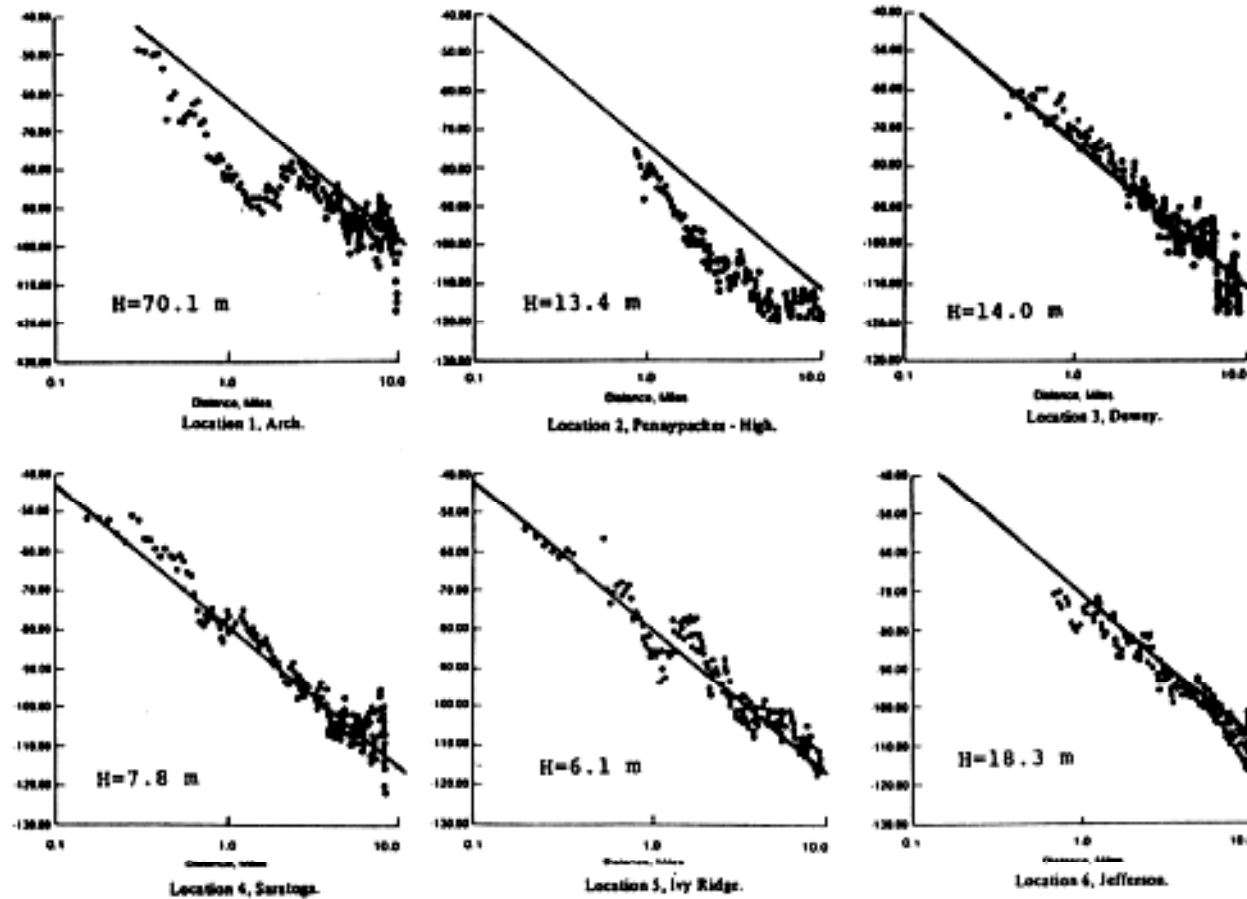


Fig. 5. Dependence of the settled field Q on the parameter $\alpha\sqrt{d}/\lambda$ with α in radians. Solid line has slope 0.9, dashed line has slope 1.0.

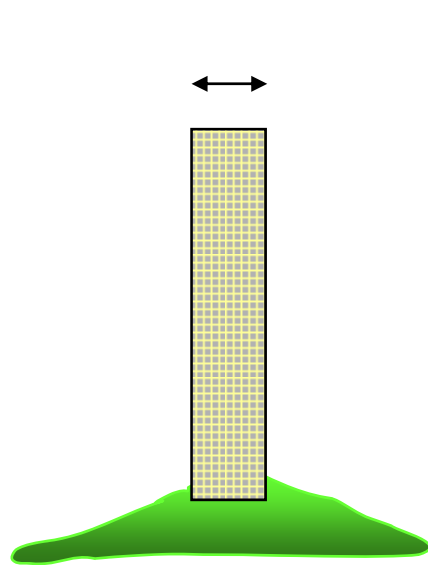
7. Macro-cells

7.4 Xia and Bertoni multi-obstacle attenuation model



8. *Advanced obstacle characterization*

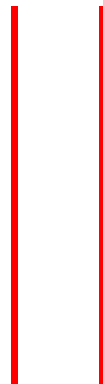
8.1 Finite depth of obstacle



① Transv. infinite knife-edge (TIKE)



② Double TI knife-edge (2-TIKE)



③ Topped 2-TIKE



8. Advanced obstacle characterization

8.1 Finite depth of obstacle

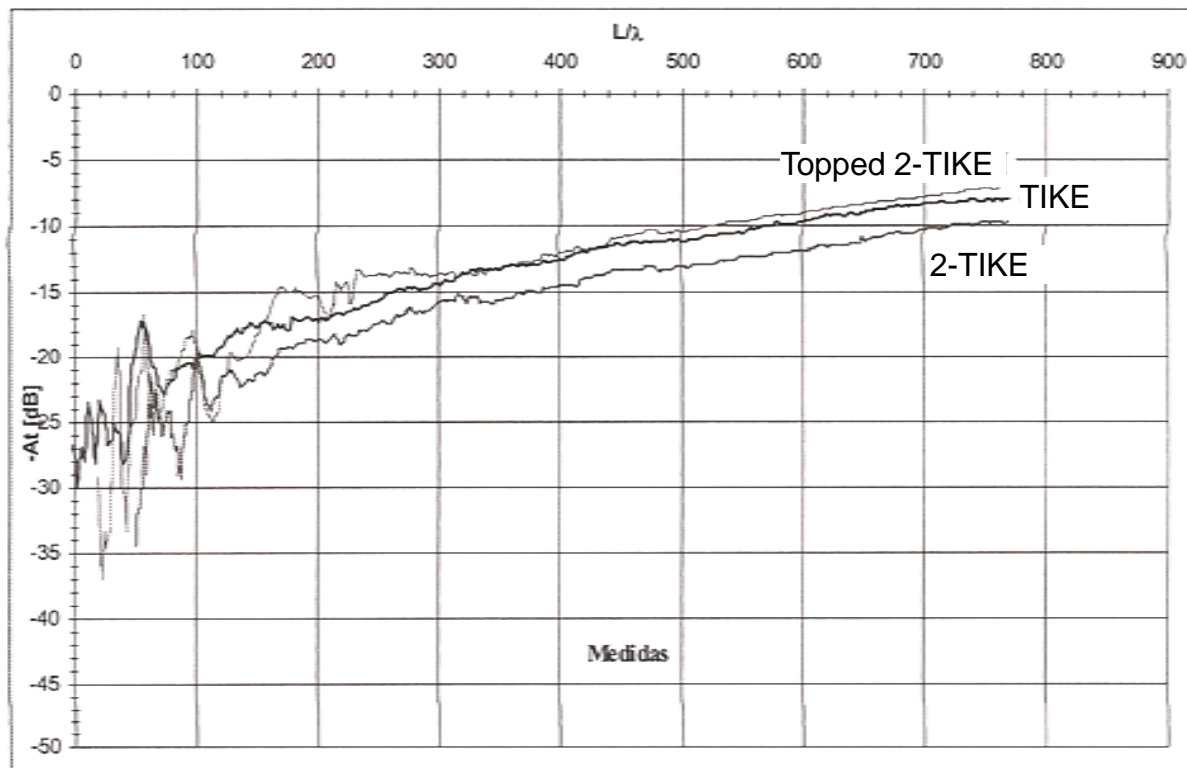
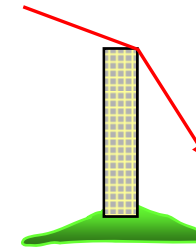


Figura 3.37 - Comparação dos valores experimentais obtidos para os vários tipos de obstáculos com a corneta piramidal como antena do móvel ($\hat{h}_0 = 350.7$)



$$\frac{x_e}{\lambda} = 8.9$$

$$\frac{x_r}{\lambda} = 37.3$$

$$\frac{d_e}{\lambda} = 137.3$$

8. Advanced obstacle characterization

8.1 Finite depth of obstacle

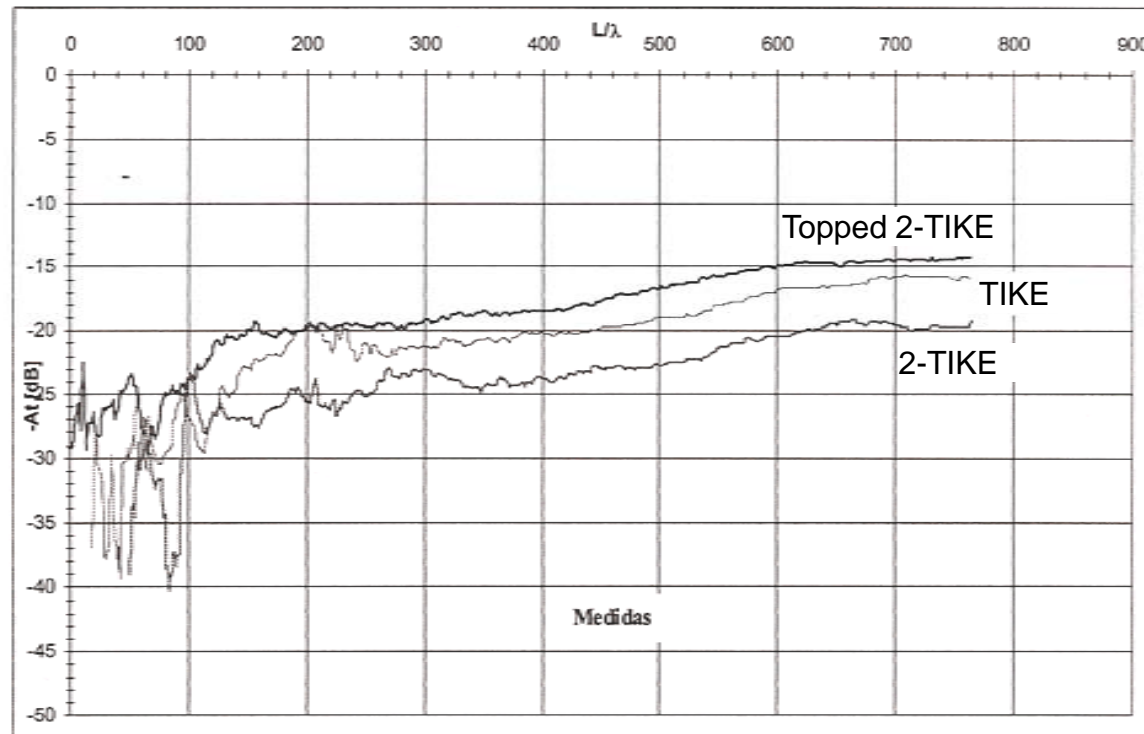
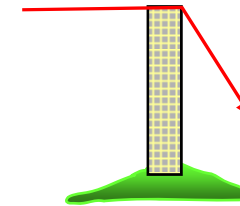


Figura 3.38 - Comparação dos valores experimentais obtidos para os vários tipos de obstáculos com a corneta piramidal como antena do móvel ($\hat{h}_0 = 341.7$)



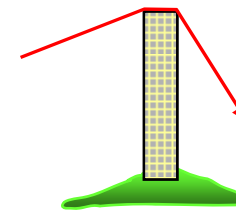
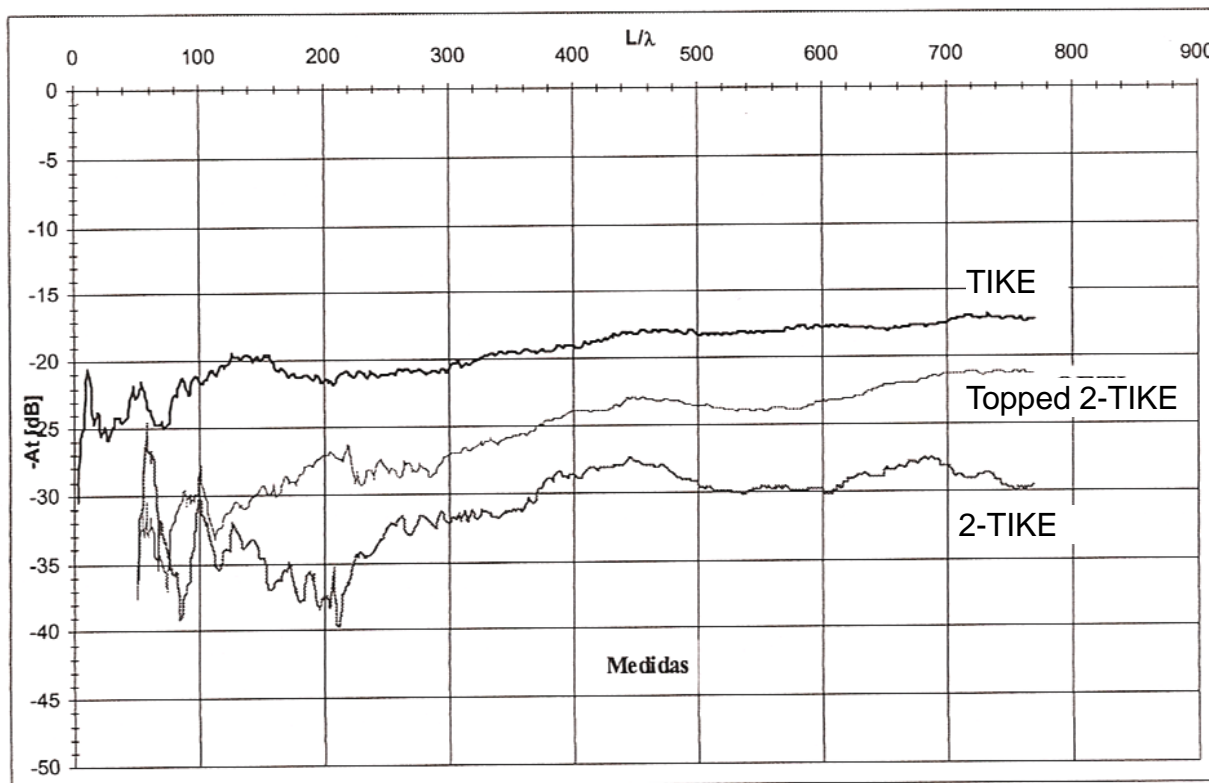
$$\frac{x_e}{\lambda} = 0$$

$$\frac{x_r}{\lambda} = 37.3$$

$$\frac{d_e}{\lambda} = 137.3$$

8. Advanced obstacle characterization

8.1 Finite depth of obstacle



$$\frac{x_e}{\lambda} = -9.0$$

$$\frac{x_r}{\lambda} = 37.3$$

$$\frac{d_e}{\lambda} = 137.3$$

8. Advanced obstacle characterization

8.2 Finite width obstacle

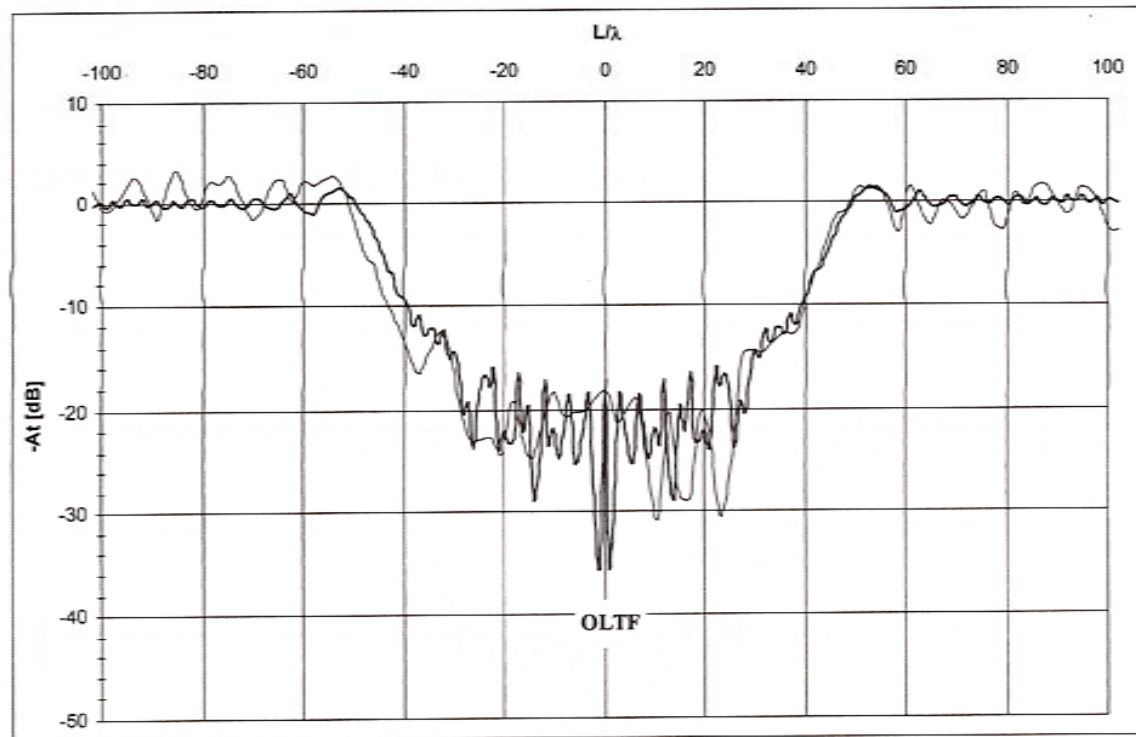
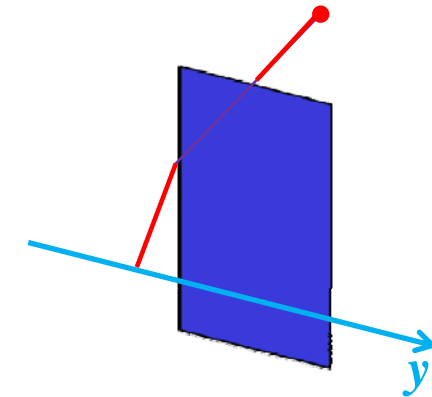


Figura 3.16 - Resultados experimentais e teóricos da atenuação suplementar introduzida por um OLTF em função do deslocamento transversal do móvel. ($\hat{x}_0 = -0.8$, $\hat{a}_1 = 88.1$)



$$\frac{x_e}{\lambda} =$$

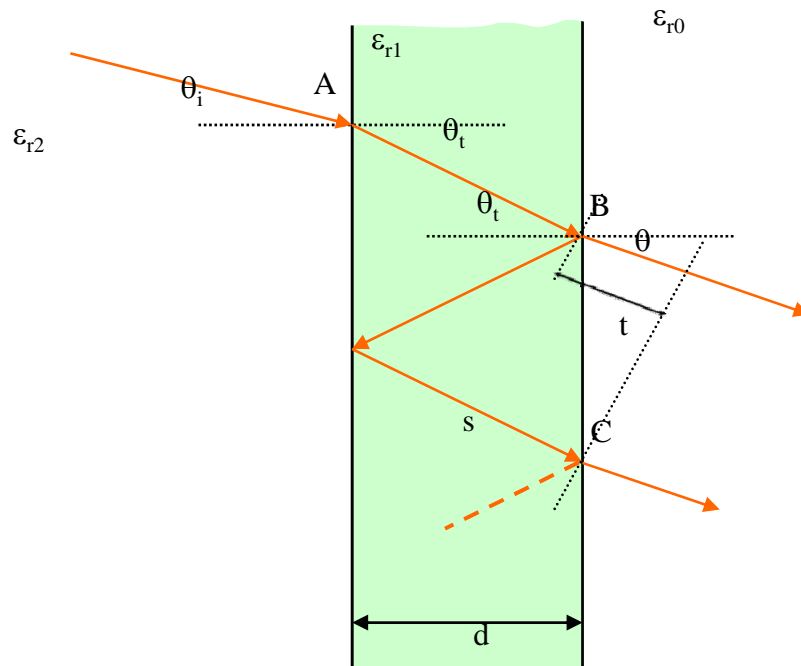
$$\frac{x_r}{\lambda} =$$

$$\frac{d_e}{\lambda} =$$

8. Advanced obstacle characterization

8.3 Through-the-wall attenuation

Generalized transmission coefficient



$$T_g = \frac{E_t}{E_i} = \frac{T_{21} T_{10} e^{-jk_0 n_1 s}}{1 - \Gamma_{10} \Gamma_{12} e^{-j2k_0 n_1 s} e^{jk_0 t}}$$

$$T_{21} = \frac{2n_{21} \cos \theta_i}{\cos \theta_i + n_{21} \cos \theta_t}$$

$$T_{10} = \frac{2n_{10} \cos \theta_t}{\cos \theta_t + n_{10} \cos \theta}$$

$$\Gamma_{10} = \frac{\cos \theta_t - n_{10} \cos \theta}{\cos \theta_t + n_{10} \cos \theta}$$

$$\Gamma_{12} = \frac{n_{21} \cos \theta_t - \cos \theta_i}{n_{21} \cos \theta_t + \cos \theta_i}$$

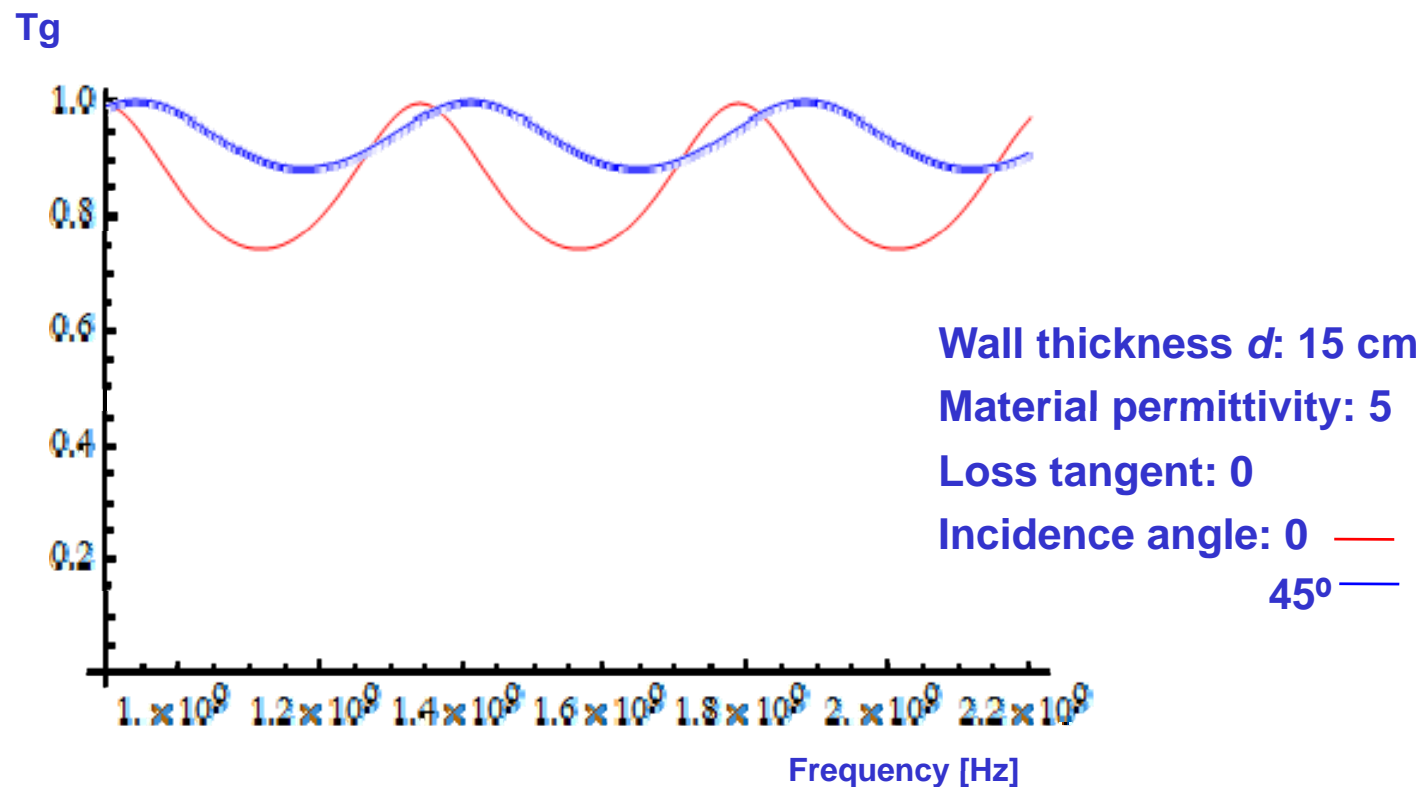
$$n_{21} = \frac{\sqrt{\varepsilon_{r2}}}{\sqrt{\varepsilon_{r1}}} = \frac{1}{n_{12}}$$

$$n_{10} = \frac{\sqrt{\varepsilon_{r1}}}{\sqrt{\varepsilon_{r0}}} = \sqrt{\varepsilon_{r1}} = n_1$$

8. Advanced obstacle characterization

8.3 Through-the-wall attenuation

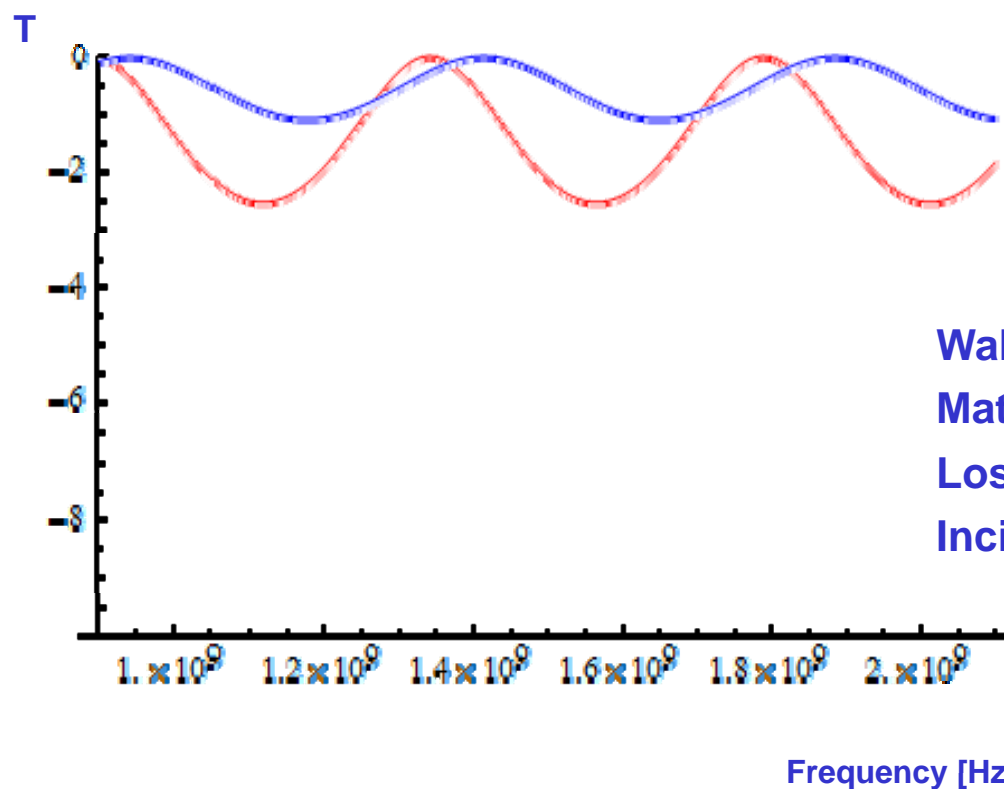
Generalized transmission coefficient (parallel polarization)



8. Advanced obstacle characterization

8.3 Through-the-wall attenuation

Transmissivity from generalized transmission coefficient (parallel polarization)



$$T = \frac{S_t \cos \theta}{S_i \cos \theta_i}$$

$$= |T_g|^2 \frac{\cos \theta}{n_2 \cos \theta_i}$$

Wall thickness d : 15 cm

Material permittivity: 5

Loss tangent: 0

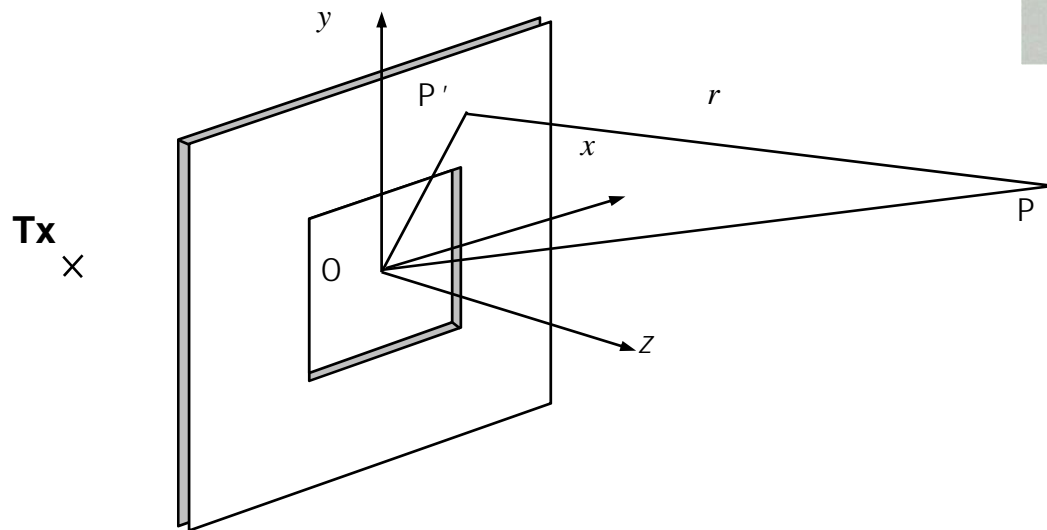
Incidence angle: 0 —

45° —

8. Advanced obstacle characterization

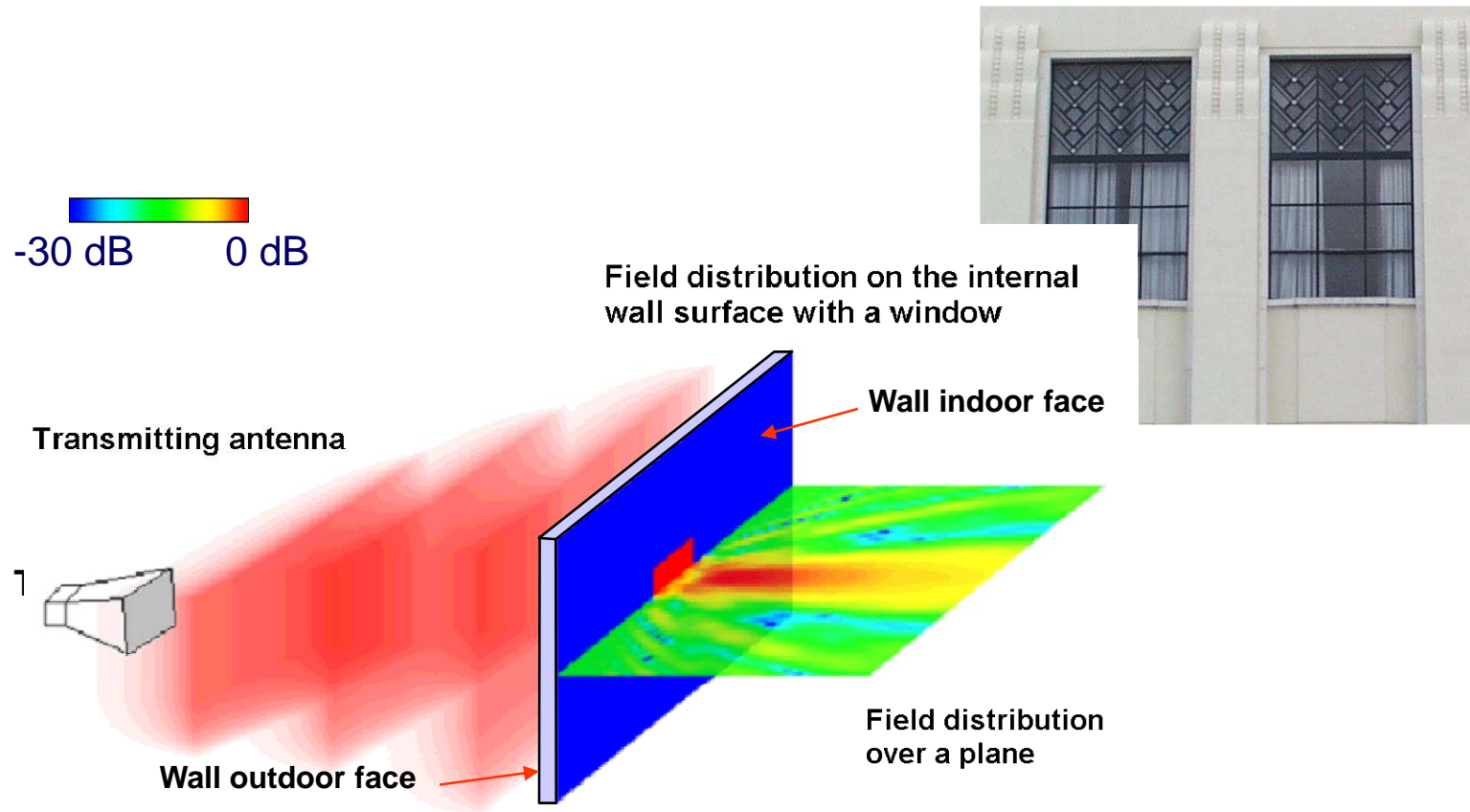
8.4 Wall with openings (windows or doors)

- Windows enhance through-the-wall transmission
- Need to quantify the influence of window size in wall transmission loss;



8. Advanced obstacle characterization

8.4 Wall with openings (windows or doors)

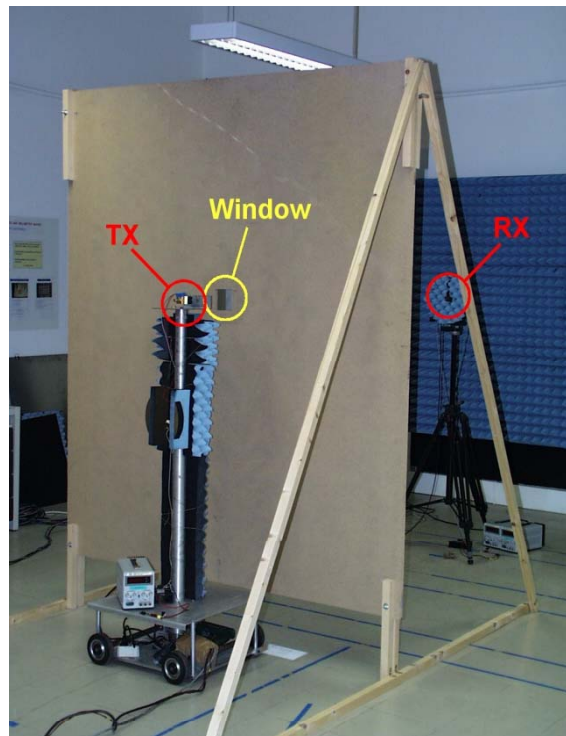


Rui Alegre; Jorge Silva – Prémio Luis Vidigal

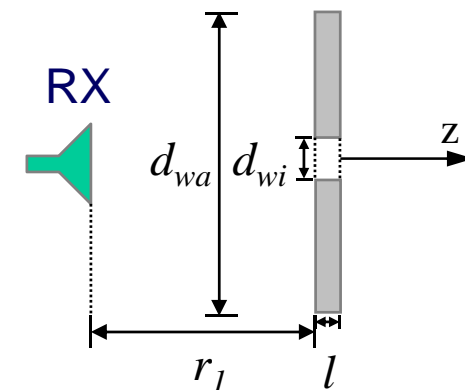
8. Advanced obstacle characterization

8.4 Wall with openings (windows or doors)

Scaled experiment for 43.0 GHz.

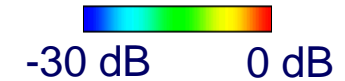


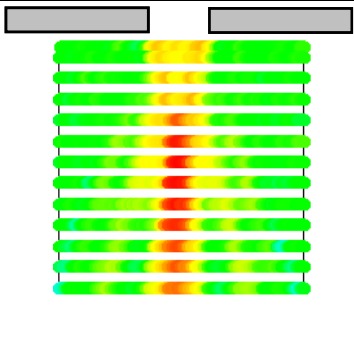
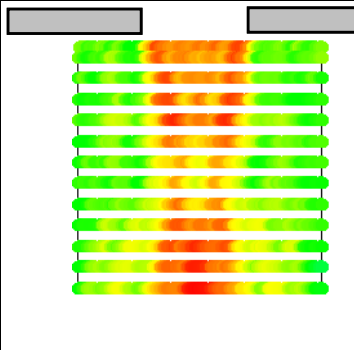
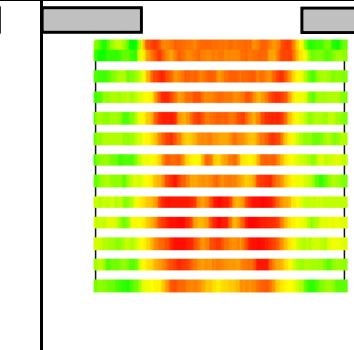
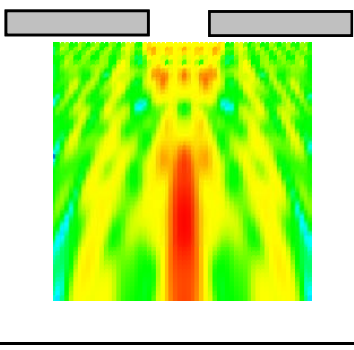
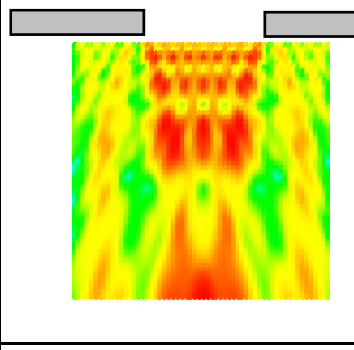
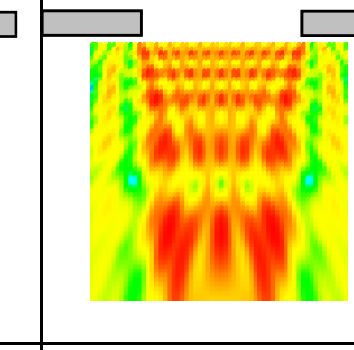
	Experimental	Simulation
f [GHz]	43.0	1.8
l [cm]	1.7	40.6
r_1 [m]	2.1	50.2
A_{wa} [m ²]	2.4×1.7	3.0×3.0
A_{ro} [m ²]	0.124×0.124	3.0×3.0



8. Advanced obstacle characterization

8.4 Wall with openings (windows or doors)

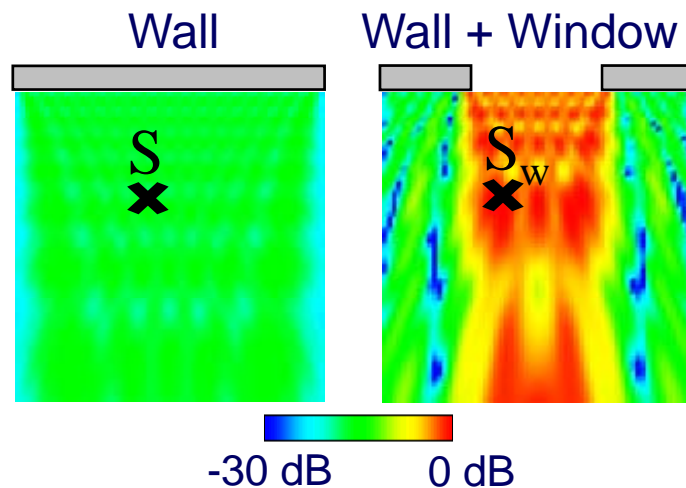


d_w [m]	0.0423	0.063	0.0887
Experimental (scaled model 43 GHz)			
Simulations			
d_w [m]	1.01	1.5	2.12

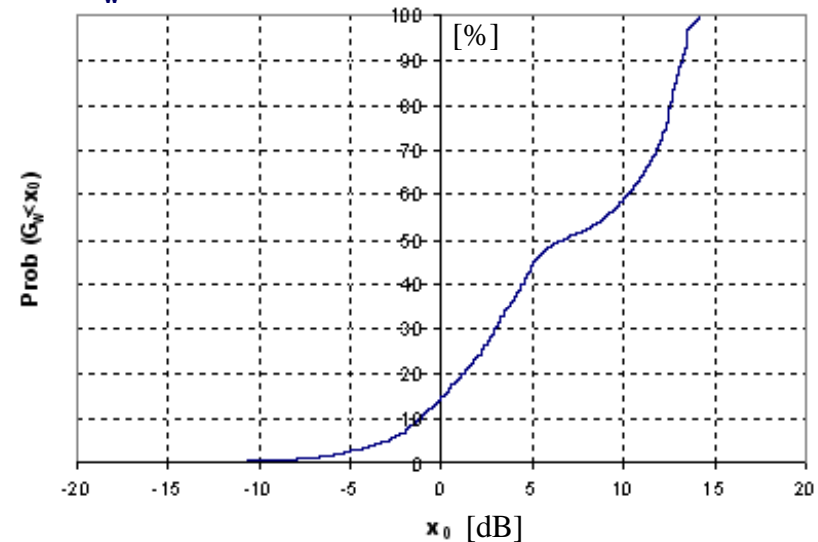
8. Advanced obstacle characterization

8.4 Wall with openings (windows or doors)

Definition of “Window Gain”: $G_w[dB] = 10\log(S_w/S)$



Fraction of room area where
 G_w is below abscissa



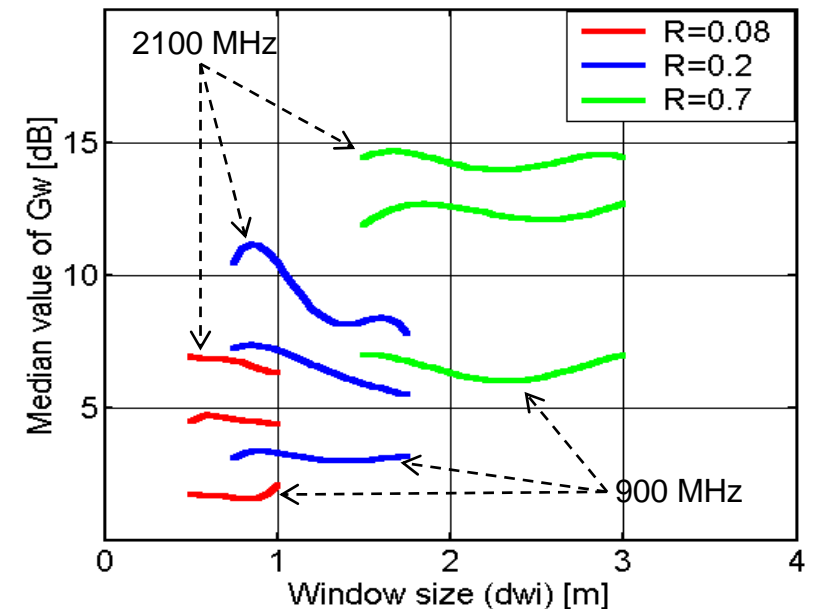
Cumulative distribution function of G_w

8. Advanced obstacle characterization

8.4 Wall with openings (windows or doors)

G_w behaviour (concrete wall)

$$R = \frac{A_{wi}}{A_{wa}} \quad \begin{array}{l} \text{(window area)} \\ \text{(wall area)} \end{array}$$



- Increasing the window size with constant R leads nearly to constant G_w (dependence only with R and f)
- G_w increases with R (at constant frequency)
- G_w increases with frequency (at constant R)